Maximum Power Point Tracking Using Kalman Filter for Photovoltaic System

Byung O Kang

Thesis submitted to the faculty of the Virginia Polytechnic Institute and State University
in partial fulfillment of the requirements for the degree of

Master of Science
In
Electrical and Computer Engineering

Douglas K. Lindner, Chairman
Dong S. Ha
William T. Baumann

December 10, 2010
Blacksburg, Virginia

Keyword: Maximum power point tracking, Kalman filter, Photovoltaic system

Maximum Power Point Tracking Using Kalman Filter for Photovoltaic System

Byung O Kang

ABSTRACT

This thesis proposes a new maximum power point tracking (MPPT) method for photovoltaic (PV) systems using *Kalman filter*. The *Perturbation & Observation* (*P&O*) method is widely used due to its easy implementation and simplicity. The *P&O* usually requires a dithering scheme to reduce noise effects, but the dithering scheme slows the tracking response time. Tracking speed is the most important factor for improving efficiency under frequent environmental change.

The proposed method is based on the *Kalman filter*. An adaptive MPPT algorithm which uses an instantaneous power slope has introduced, but process and sensor noises disturb its estimations. Thus, applying the *Kalman filter* to the adaptive algorithm is able to reduce tracking failures by the noises. It also keeps fast tracking performance of the adaptive algorithm, so that enables using the *Kalman filter* to generate more powers under rapid weather changes than using the *P&O*.

For simulations, a PV system is introduced with a 30kW array and MPPT controller designs using the *Kalman filter* and *P&O*. Simulation results are provided the comparison of the proposed method and the *P&O* on transient response for sudden system restart and irradiation changes in different noise levels. The simulations are also performed using real irradiance data for two entire days, one day is smooth irradiance changes and the other day is severe irradiance changes. The proposed method has showed the better performance when the irradiance is severely fluctuating than the *P&O* while the two methods have showed the similar performances on the smooth irradiance changes.

Dedication

I dedicate this thesis to my beloved family who always love and support me to pursue this degree.

Acknowledgement

I am heartily thankful to my off-campus advisor, Dr. Jae H. Park, whose encouragement, guidance and support from the initial to the final level enabled me to develop an understanding of the research. I would also like to acknowledge the support of my committee chairman, Dr. Douglas K. Lindner. I also thank to my committee members, especially Dr. William T. Baumann for his advice on editing this thesis.

I would like to thank to Eunju Woo for supporting and encouraging me to pursue this degree. Special thanks also to all my friends in Blacksburg, especially Suwan Myung for supporting me since studying together in Korea and Jaesung Jung for achieving solar irradiance data.

I wish to express my love and gratitude to my beloved family; for their support and endless love, through the duration of my studies.

Table of Contents

Chapter 1. Introduction 1
1.1 Photovoltaic System 1
1.2 Maximum Power Point Tracking 2
1.3 Kalman Filter 4
1.4 Thesis Motivation 5
Chapter 2. Review of Literature 9
2.1 PV Array Characteristics 9
2.1.1 Equivalent Circuit 9
2.1.2 Graphs of Characteristics 11
2.2 Present MPPT Methods 12
2.3 Perturbation & Observation Method 12
2.3.1 Algorithm 13
2.3.2 Tracking Failure under Rapid Environmental Change 14
2.4 Noise Reduction: Dithering 15
Chapter 3. Proposal of New MPPT Method 17
3.1 General Description of Kalman Filter 17
3.2 Noise Analysis 18
3.3 Proposed Representation 19
3.3.1 Adaptive MPPT Algorithm 19
3.2.3 Proposal of New Representation 21
3.4 Applied Proposed Representation to Kalman Filter 23
3.3.2 Time Update 24
3.3.3 Operating Summary in Proposed Method 24
Chapter 4. PV System Design 26
4.1 Assumptions 26
4.2 Array Design 27
4.3 Oscillation in Steady-State 28
4.4 Design of Proposed Method 30
4.4.1 Parameter Selection 30
4.4.2 Performance Verification of Kalman Filter 33
4.5 Design of P&O Method 35
Chapter 5. Simulations 37
5.1 Transient Response to Sudden Changes 38
5.1.1 Sudden System Restart 39
5.1.2 Sudden Irradiance Changes 41
5.1.3 Summary of Sudden Changes 44
5.2 Daily Generation 46
5.2.1 Smooth Irradiance Changes 47
5.2.2 Severe Irradiance Changes 49
5.2.3 Summary of Daily Generation 53
Chapter 6. Conclusion and Future Works 55
6.1 Conclusion 55
6.2 Future Works 56
Chapter 7. References 57

List of Figures

Figure 1.1: Block diagram of PV system 1
Figure 1.2: (a) I-V characteristic and (b) P-V characteristic of PV panel 2
Figure 1.3: Irradiance dependence of P-V characteristic 3
Figure 1.4: Temperature dependence of P-V characteristic 3
Figure 1.5: *Kalman filter* (estimator) diagram 4
Figure 1.6: Example of *Kalman filter* – GPS system 5
Figure 1.7: Daily irradiance data between March 1 and March 15, 2009 7
Figure 1.8: Daily irradiance data between March 16 and March 30, 2009 8
Figure 2.1: PV array equivalent circuit 9
Figure 2.2: (a) Temperature and (b) irradiance dependence of *HIP-200BA19*'s I-V characteristic 11
Figure 2.3: Flowchart of *P&O* method 13
Figure 2.4: *P&O*'s tracking failure under sudden P-V characteristic change 14
Figure 2.5: Example of dithering scheme using triangular waves 15
Figure 2.6: Comparison of using and not using dithering in *P&O* 16
Figure 3.1: Block diagram of operation of MPPT in PV system 20
Figure 3.2: Controlling errors between actual voltage (V_{act}) and reference voltage (V_{ref}) 21
Figure 4.1: P-V characteristic of designed array at 25°C and 1 kW/m^2 28
Figure 4.2: Linear and nonlinear regions of P-V characteristic 31
Figure 4.3: Power slope calculations based on Figure 4.1 32
Figure 4.4: Tracking direction in P-V characteristic at 25°C and 1 kW/m^2 33
Figure 4.5: Simulation result of using designed *Kalman filter* and equation (3.14) following Figure 4.4 34
Figure 4.6: Average power values of 500 simulations following Figure 4.4 34
Figure 4.7: Tracking result following Figure 4.4 using designed *P&O* method 36
Figure 5.1: Initial 120 estimation results of proposed method in sudden system restart 39
Figure 5.2: Simulation result of sudden system restart under 60dB process noise 40
Figure 5.3: Simulation result of sudden system restart under 80dB process noise 40
Figure 5.4: Simulation result of sudden system restart under 40dB process noise 41
Figure 5.5: Middle 200 estimation results of proposed method before and after irradiance change 42
Figure 5.6: Simulation result of 50% decrease of irradiance under 60dB process noise 43
Figure 5.7: Simulation result of 50% decrease of irradiance under 80dB process noise 43
Figure 5.8: Simulation result of 50% decrease of irradiance under 40dB process noise 44
Figure 5.9: Example of difference between 1-min interval and interpolated irradiance data 46
Figure 5.10: Irradiance data on March 14, 2009 47
Figure 5.11: Simulation results of daily generation on March 14, 2009 48
Figure 5.12: Simulation results limited to between 6:15 AM and 6:30 AM on March 14, 2009 49
Figure 5.13: Irradiance data on March 25, 2009 50
Figure 5.14: Simulation results of daily generation on March 25, 2009 51
Figure 5.15: Simulation results limited to between 10:45 AM and 11:15 AM on March 25, 2009 52

List of Tables

Table 3.1: Measurement and time updates in general *Kalman filter* 18
Table 3.2: Measurement and time updates in proposed *Kalman filter* 25
Table 4.1: Electrical specification of *Sanyo HIP-200BA19* 27
Table 5.1: Transient response comparison of two methods in each scenario and noise level 45
Table 5.2: Generated power comparison of two methods over 1-min in each scenario ... 45
Table 5.3: Generated power comparison of two methods in each day based on 1-min interval data 53
Table 5.4: Generated power comparison of two methods in each day based on interpolated data 53
Table 5.5: Expected cost advantage of proposed method per day (Denmark & U.S.) 54

Chapter 1
Introduction

1.1 Photovoltaic System

As fossil energy becomes more expensive and causes growing environmental concerns, energy from natural resources such as sunlight and wind are globally welcomed to replace the fossil fuel. Among methods of generating electric power by alternative resources, photovoltaic (PV) has grown steadily in recent decades as a carbon-free technology alternative [1].

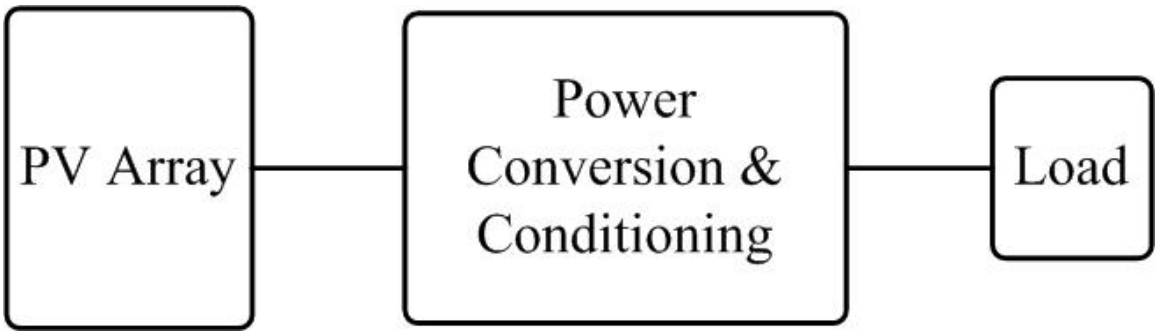

Figure 1.1: Block diagram of PV system

PV converts sunlight directly into current electricity by means of the photovoltaic effect. Since common solar cells are made from silicon-based semiconductors, the photovoltaic effect is involved with the p-n junction of the solar cells. First, sunlight produces electron-hole pairs (EHPs) into the cell. Then, the electrons move to the n-region and the holes move to the p-region as a result of the electric field created by the junction. The electric charges collected in both regions finally flow as electric current into a connected load [2].

A PV system is a power system that generates direct current (DC) from sunlight and processes it requiring DC or alternating current (AC) electricity. Instead of solar cells,

the PV system generally uses PV panel-interlinked packages with solar cells-or PV arrays-combined assemblies of PV panels-due to the low voltage of a single solar cell. As shown in Figure 1.1, the PV system consists of three stages: power generation, power conversion & conditioning, and power distribution. In the power generation stage, the PV array generates DC electricity directly from sunlight. The generated DC must be controlled and conducted in the power conversion & conditioning stage to suit distribution requirements. This stage uses power electronic devices such as DC-DC converters and/or DC-AC inverters for processing DC from the array. The system is classified into stand-alone and grid-tie according to the load connection. The output electricity from the power conversion & conditioning stage is fed into the grid in the grid-tied while the electricity is stored in a battery or used by an electric device directly in the stand-alone [1].

1.2 Maximum Power Point Tracking

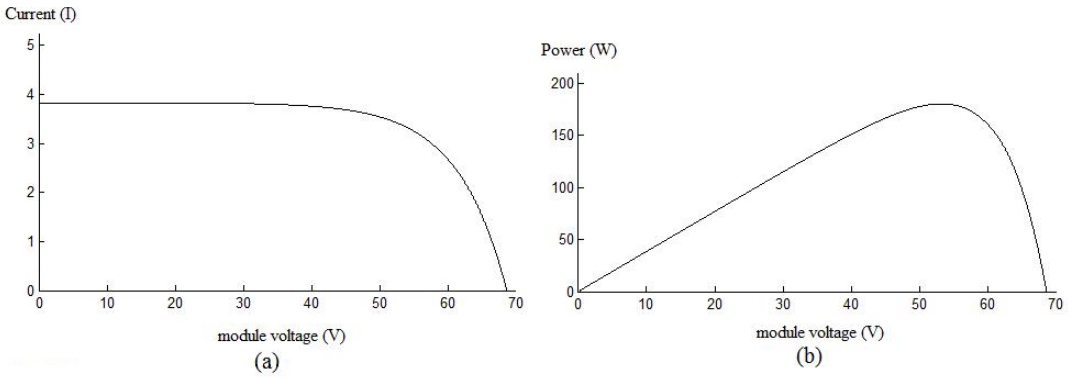

Figure 1.2: (a) I-V characteristic and (b) P-V characteristic of PV panel

The output current of PV panels varies depending on the status of the load. Figure 1.2(a) and (b) are current (I)-voltage (V) and power (P)-voltage (V) characteristics of a certain PV panel respectively. Over a wide range of I and V, it is very essential to find a point that maximizes the output power. The power is calculated by product of V and I. The point maximizing the power consequently enables for users to extract maximum capable power from the PV cell. The point is called the Maximum Power Point (MPP)

and finding this point is called Maximum Power Point Tracking (MPPT). Here tracking does not mean physical movement e.g., following on the sun.

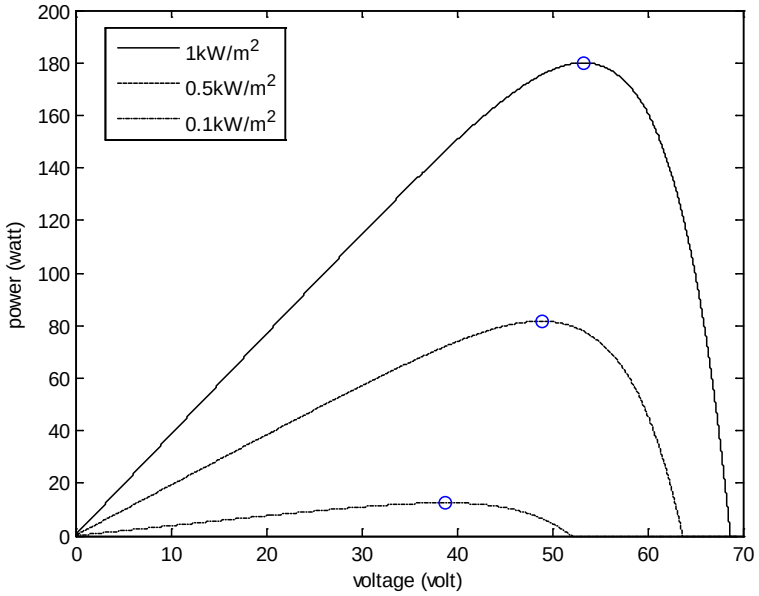

Figure 1.3: Irradiance dependence of P-V characteristic

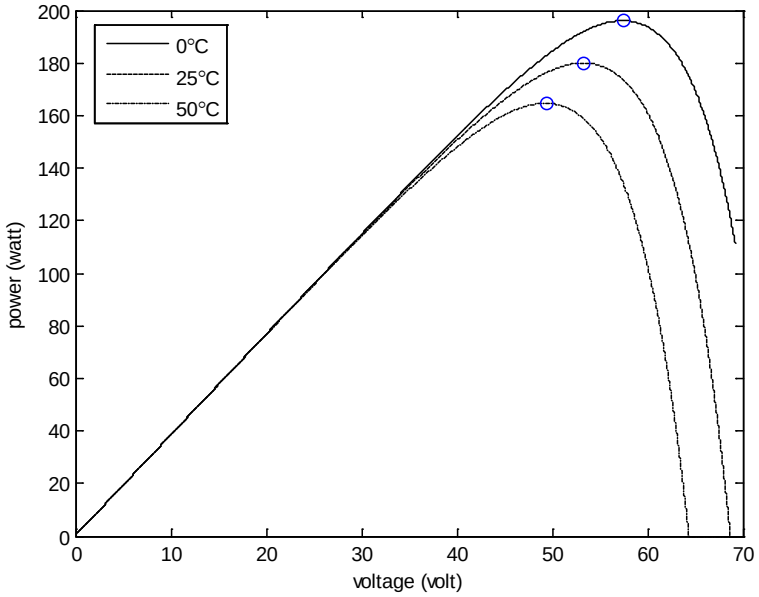

Figure 1.4: Temperature dependence of P-V characteristic

Figure 1.3 and 1.4 are different P-V characteristics of a certain panel as different irradiances and temperature respectively. The circles represent a single MPP in each characteristic. As the P-V characteristic is constantly varying by changing the irradiance

and temperature, the MPP must be tracked at the changed moment to maximize the output power from the panel. Therefore, both a tracking speed and accuracy are required to the PV system. The MPPT performance may be considered as an important factor to increase generation revenue.

1.3 Kalman Filter

The *Kalman filter* is a well-known computational tool which provides stochastic estimation in a noisy environment. Rudolph E. Kalman introduced his recursive approach to solve a linear filtering problem in 1960. The *Kalman filter* operates on estimating states by using recursive time and measurement updates over time [3]. More details related to the updates are explained in Chapter 2. These recursive cycles allow for a decrease in the noise effect in a system, which consequently tends to approach the true values of the measurements. The *Kalman filter* is well suited to use for a digital design because its direct processing ability in time domain is suitable to computer-based calculation [4].

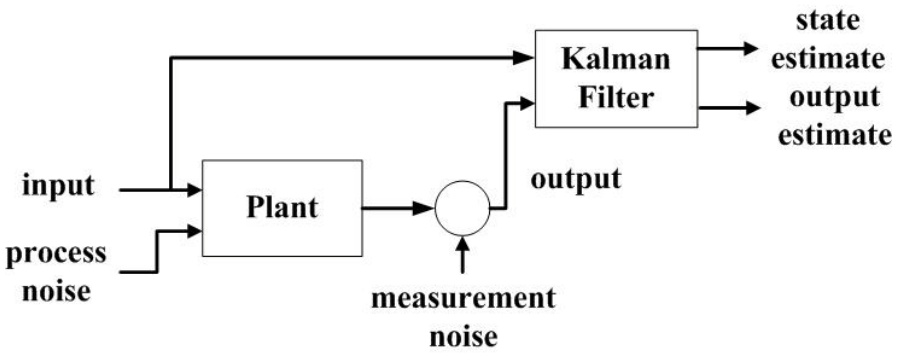

Figure 1.5: *Kalman filter* (estimator) diagram [5]

The *Kalman filter* is sometimes called to the *Kalman* estimator. As shown in Figure 1.5, the *Kalman filter* generates state and output estimates from input and output with filtering the noises. A literal role of 'filter' is reducing the noises contained in the two input signals of the filter, but the *Kalman filter* is eventually used for estimating the

state. Therefore, it has an efficient performance for estimating the state in a dynamic system in a noisy environment [3, 6]

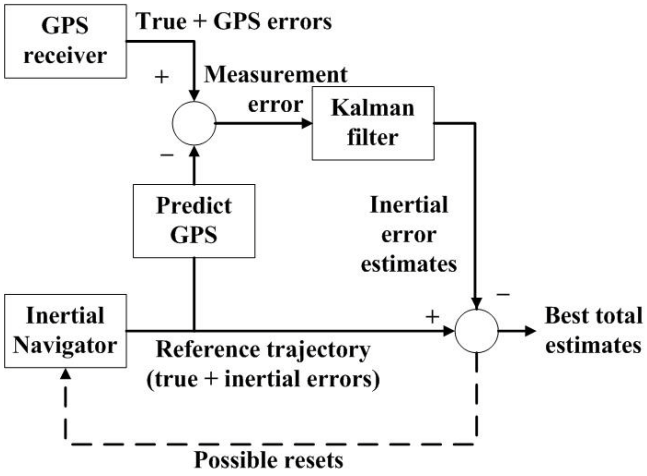

Figure 1.6: Example of *Kalman filter* – GPS system [7]

The *Kalman filter* had developed to apply for tracking spacecrafts and missiles, but the applications of the *Kalman filter* are numerous currently: global positioning system (GPS), image vision system, robotics, weather forecasting, economics, and etc, as well as tracking objects [3, 8-10]. Figure 1.6 is an example of the *Kalman filter* used for a GPS system. The *Kalman filter* improves the system's performance by estimating an inertial error, which is a state in the system, based on errors between real positioning data from a GPS receiver and a reference trajectory from an inertial navigator. Since the positioning data include errors, the *Kalman filter* reduces the GPS errors and estimates the accurate inertial error. The system consequently produces the best estimation from a comparison between the reference trajectory and the estimated inertial error.

1.4 Thesis Motivation

This thesis proposes a new MPPT method using *Kalman filter* in a PV system. The proposed MPPT is controlled by microcontroller-based power electronic devices in the PV system.

A practical outdoor PV system is dependent on time-varying temperature and irradiance. All plots in Figure 1.7 and 1.8 show daily irradiance changes in an identical location between March 1 and March 30, 2009. Irradiance data and plots are utilized from the Solar Radiation Research Laboratory BMS (SRRL BMS) which is located in Golden, Colorado, longitude 105.18 degree west and latitude 39.74 degree north [11]. From observing the plots over 30 days, there are sharp irradiance changes for some moments in a day or for an entire day except of 4 days: March 5, 8, 11, and 14. The exceptional 4 days are assumed as a suitable environmental condition for the PV generation. A transient response of a MPPT controller is not a considerable factor in performance specifications in those days. For the other 26 days, contrarily, I-V and P-V characteristics of a connected PV array are changed continuously and momentarily for the limited time in the day or for the entire day, and the MPPT controller is required to track on MPPs quickly whenever the characteristics are changed.

Present power electronic devices use a microcontroller or digital signal processor (DSP) as a controller, and MPPT is performed by the same controller. However, the power electronic devices contain various noises e.g., switching noise, thermal noise, and etc. In addition, a voltage and current sensors are used to achieve voltages and current data from the array, but the sensors have errors from an accuracy specification and analog-to-digital converter (ADC) quantization. As the above noises and errors may degrade the tracking performance, the MPPT controller is required to be robust against the noises and errors.

Consequently, the MPPT using by the *Kalman filter* is an alternative to expect an acceptable performance against both the noises and dynamic environmental condition changes. Due to the estimation ability of the *Kalman filter* in the dynamic system with the noisy environment, the accurate MPP can be predicted by the *Kalman filter* without any drop of system dynamics; other MPPT methods sometimes lose their system dynamics partially to eliminate the noise effects. High computing amount of the *Kalman filter* may be considered to a disadvantage. However, the present commercial microcontroller or DSP has from hundreds of megahertz (MHz) to a gigahertz (GHz). Those speeds may be assumed to overcome the *Kalman filter*'s computations with several hundreds of hertz (Hz) speed of the MPPT controller.

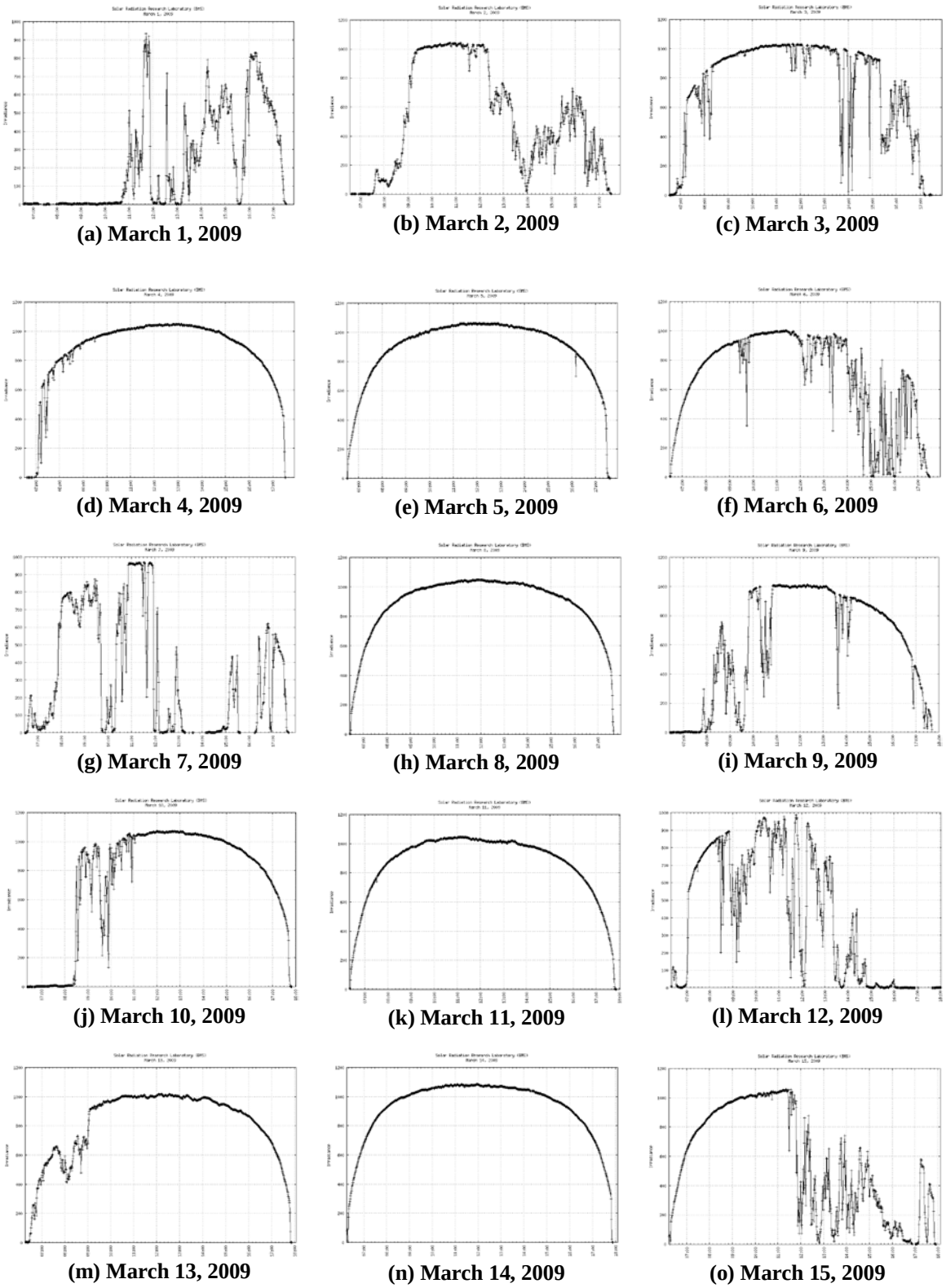

(a) March 1, 2009 (b) March 2, 2009 (c) March 3, 2009

(d) March 4, 2009 (e) March 5, 2009 (f) March 6, 2009

(g) March 7, 2009 (h) March 8, 2009 (i) March 9, 2009

(j) March 10, 2009 (k) March 11, 2009 (l) March 12, 2009

(m) March 13, 2009 (n) March 14, 2009 (o) March 15, 2009

Figure 1.7: Daily irradiance data between March 1 and March 15, 2009

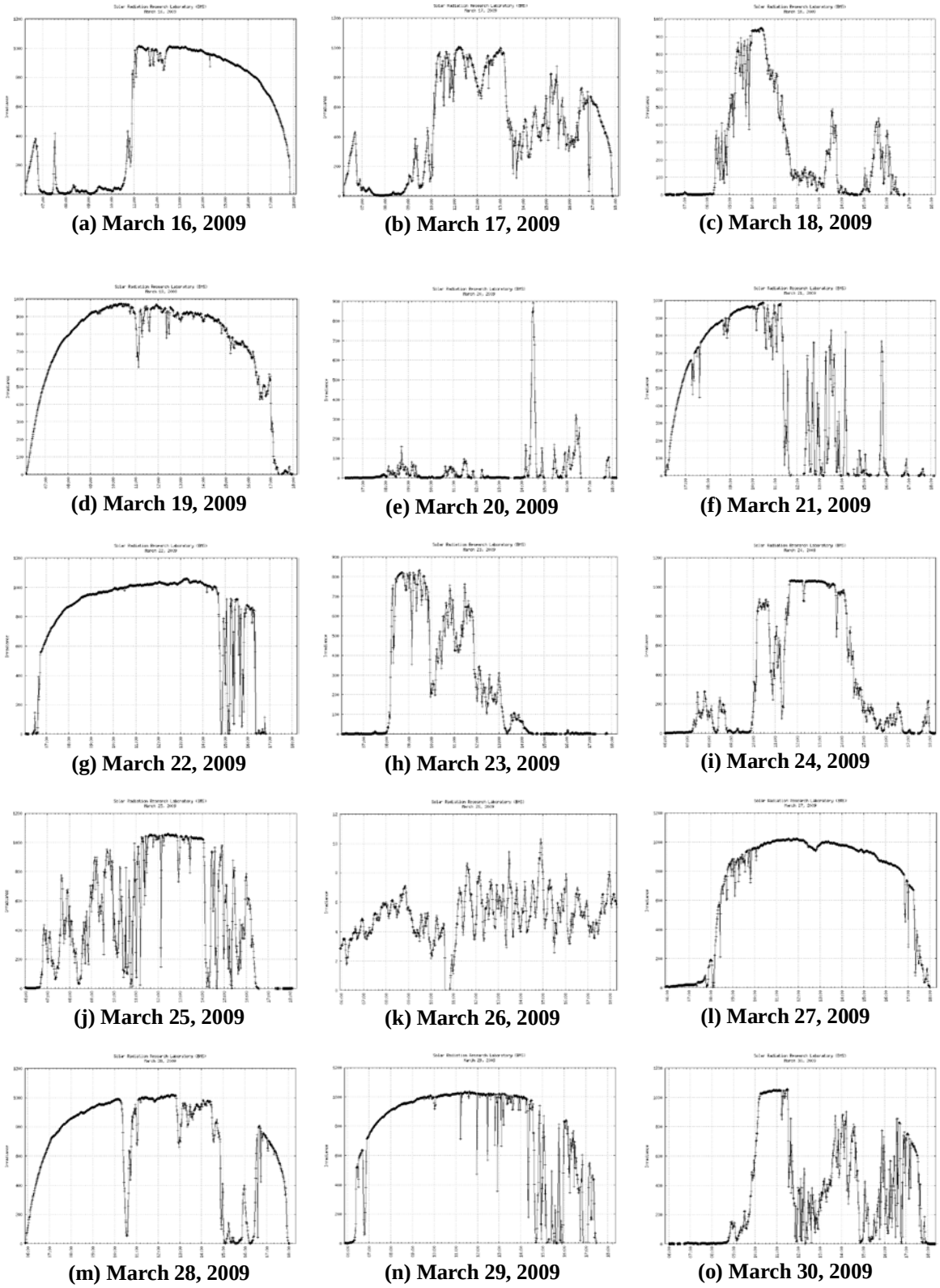

(a) March 16, 2009 **(b) March 17, 2009** **(c) March 18, 2009**

(d) March 19, 2009 **(e) March 20, 2009** **(f) March 21, 2009**

(g) March 22, 2009 **(h) March 23, 2009** **(i) March 24, 2009**

(j) March 25, 2009 **(k) March 26, 2009** **(l) March 27, 2009**

(m) March 28, 2009 **(n) March 29, 2009** **(o) March 30, 2009**

Figure 1.8: Daily irradiance data between March 16 and March 30, 2009

Chapter 2
Review of Literature

2.1 PV Array Characteristics

2.1.1 Equivalent Circuit

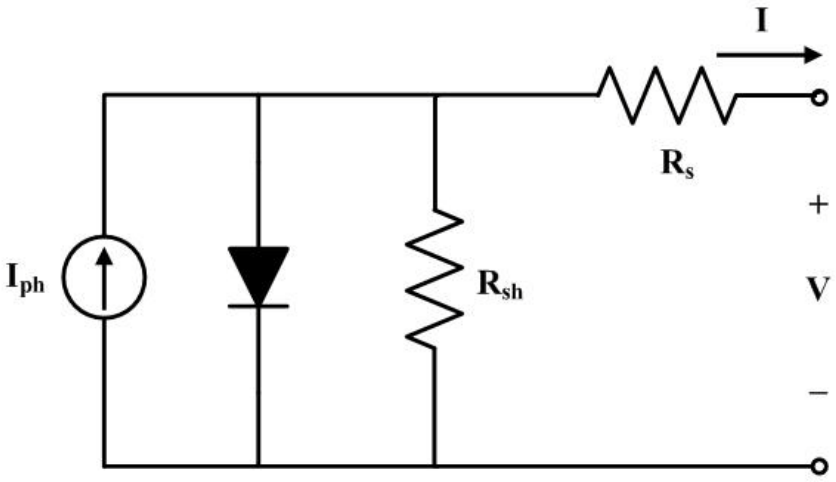

Figure 2.1: PV array equivalent circuit

Figure 2.1 shows the typical equivalent circuit for PV arrays. In general, the series parasitic resistance R_s is very small and the parallel parasitic resistance R_{sh} is very large; they are negligible [12]. Then, the output current I can be expressed by:

$$I = I_{ph} - I_O\left[\exp\left(\frac{qV}{nkT}\right) - 1\right] \tag{2.1}$$

V is the output voltage of the cell. λ is the irradiance in kW/m^2, and T is the temperature in K. q is the elementary charge ($=1.6\times10^{-19}\,C$), and k is the Boltzmann's constant

($=1.38\times10^{-23}\,J/K$). n is the diode factor. I_O is the reverse saturation current in amperes. The short-circuit current (I_{SC}) and the open-circuit voltage (V_{OC}) are calculated in the following:

$$I_{ph} = I_{SC} \text{ where } V = 0\ ,\ I = I_{SC} \tag{2.2}$$

$$I_O = \frac{I_{SC}}{\exp\left(\frac{qV_{OC}}{nkT}\right)-1} \text{ where } I = 0\ ,\ V = V_{OC}\,. \tag{2.3}$$

The photocurrent I_{ph} is achieved following:

$$I_{ph} = I_{SC}^{\ *} \cdot \lambda \tag{2.4}$$

where $I_{SC}^{\ *}$ is the short-circuit current when T is 25°C and λ is 1 kW/m^2 [2]. The equation (2.4) explains that the photocurrent is proportional to the irradiance.

In practice, however, above equations include uncertain values. Therefore, [13] suggested the simplified equation of the output current with only one uncertain parameter A following:

$$I = I_{ph} - \frac{I_{SC}^{\ *}}{\exp\left(\frac{q}{kT}A\right)}\left[\exp\left(\frac{q}{kT}A\frac{V}{V_{OC}}\right)-1\right] \text{ where } A = 0.2464 \tag{2.5}.$$

[13] also showed the comparison between the characteristics using the equation (2.5) and a real experiment. As the result, the electrical features of (2.5) with a specific A=0.2464 illustrates strong similarity to that of the real experiment.

2.1.2 Graphs of Characteristics

From the equation (2.4) and (2.5), temperature and irradiance are dominant factors for deciding the relationship between the output current and voltage of the cell. Figure 2.2(a) and (b) include the I-V characteristics of a certain PV panel-*Sanyo HIP-200BA19*- respectively under various temperatures and irradiances. Figure 2.2(a) shows the temperature dependence of the I-V characteristic of *Sanyo HIP-200BA19*. As temperature increases, the overall voltage range of the cell is decreasing. This feature indicates that the voltage of the MPP decreases with increasing temperature. Figure 2.2(b) shows the irradiance dependence of the I-V characteristic of *Sanyo HIP-200BA19.* Under higher irradiance, the PV cell produces higher output currents because the current is proportionally generated by the flux of photons [14]. This feature also explains that the current of the MPP decreases with decreasing irradiance. Since decreasing either currents or voltages reduces output power, lower temperature and higher irradiance are required to get more power under the same panel. In addition, the irradiance has a much greater effects on changing the panel characteristics than does the temperature. When the temperature drops 50% from 50°C to 25°C, the panel voltage is increased about 10%. However, 50% change of the irradiance from 1 kW/m^2 to 0.5 kW/m^2 causes a reduction of the panel current by 50%.

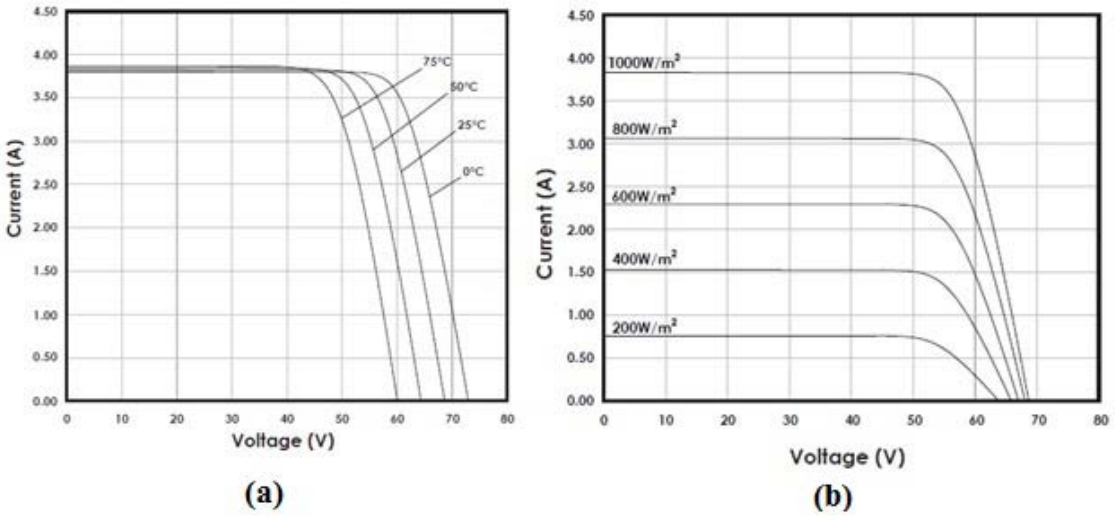

Figure 2.2: (a) Temperature and (b) irradiance dependence of *HIP-200BA19*'s I-V characteristic [15]

2.2 Present MPPT Methods

Since MPPT is a key step in increasing energy efficiency in PV systems, many MPPT methods have been proposed over decades. According to Esram et al, the number of MPPT papers per year is generally growing since 1968, and last decade particularly shows significant growth rate [16]. It is also indicated that recent papers tend to repeat or slightly modify conventional ideas [16]. This suggests that frequently mentioned techniques have effective algorithms.

More than 11 methods are introduced by Esram et al,: *Hill Climbing/Perturbation & Observation (P&O),Incremental Conductance (IncCond), Fractional Open-Circuit Voltage, Fractional Short-Circuit Current, Fuzzy Logic Control, Neural Network, Ripple Correlation Control (RCC), Current Sweep, DC-Link Capacitor Droop Control, Load Current or Voltage Maximization, dP/dV or dP/dI Feedback Control, and etc* [16]. Among the methods, the *P&O* and *IncCond* are most popular methods for several reasons. The first is that the two methods can be easily applied to a microcontroller- or DSP-based design because both algorithms are very simple. Secondly, they are both independent of PV arrays; users have the flexibility to choose arrays. Indeed, both algorithms are based on tracking real MPPs. It means both are expected to have accurate tracking performance under any environmental condition compared to other methods which are not tracking real ones. Because of these reasons, these two methods are popularly used to implement as a MPPT method in industry.

2.3 Perturbation & Observation Method

The *Perturbation & Observation (P&O)* has been used mostly for its simplicity and easy implementation [16, 17]. It can be applied to both analog and digital designs. It is also compatible with any kind of PV arrays [13]. Therefore, the *P&O* is frequently applied to digital designs although it was initially developed for analog designs.

2.3.1 Algorithm

The *P&O* is based on a comparison of perturbation voltage and changed power. As shown in Figure 2.3, the *P&O* controller first measures voltage *V(k)* and current *I(k)* of a PV array at time *k* through voltage and current sensor. It also calculates power *P(k)* by the product of *V(k)* and *I(k)*. And then, the controller compares between the present power *P(k)* and previous power *P(k-1)*, and between the present voltage *V(k)* and previous voltage *V(k-1)*. If both voltage perturbation ΔV and changed power ΔP are positive or negative together, next voltage perturbation must be positive because the present point is located on the left side of the MPP. If one is positive and the other is negative, next perturbation must be negative because the point is on the right of the MPP. Theoretically the MPP is when ΔP is zero; the derivative $\Delta P/\Delta V$ is zero. The *P&O* use PV array voltage as perturbation while the *Hill Climbing* uses a duty ratio of a power converter [16].

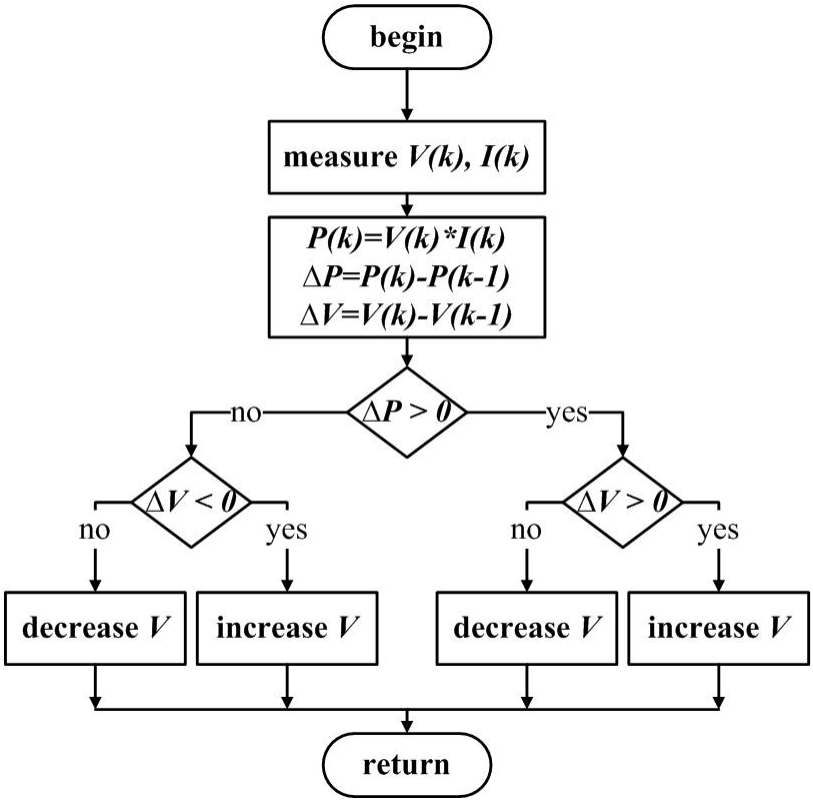

Figure 2.3: Flowchart of *P&O* method

2.3.2 Tracking Failure under Rapid Environmental Change

However, the *P&O* sometimes shows tracking failure under rapid environmental condition changes [16, 17]. As illustrated in Figure 2.4, let us suppose that the P-V characteristic C_1 is suddenly shifted to C_2 because of an environmental change. Under the constant C_1, the MPP point M_1 must move to P_1 by a positive perturbation step +dV, and then it would come back to M_1 by a negative perturbation step –dV at as the result of comparing powers at between M_1 and P_1. However, the M_1 will move to P_2 due to the changed characteristic C_2. In this case, the next perturbation must be negative for moving from P_2 to M_2, but P_2 will jump oppositely to P_3 due to the positive perturbation +dV. The *P&O* controller orders the positive perturbation as the result that the power at P_2 is still higher than the power at M_1. This phenomenon disturbs the controller to track toward the new MPP immediately when the environmental condition is changed.

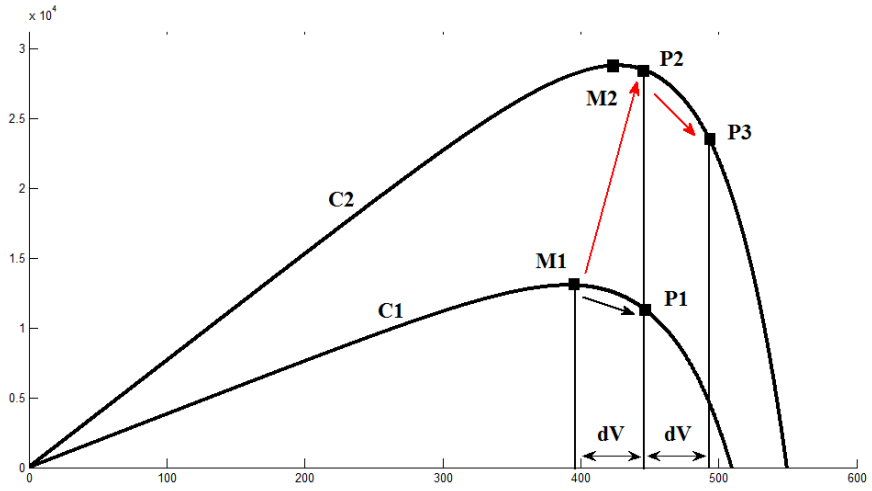

Figure 2.4: *P&O*'s tracking failure under sudden P-V characteristic change

2.4 Noise Reduction: Dithering

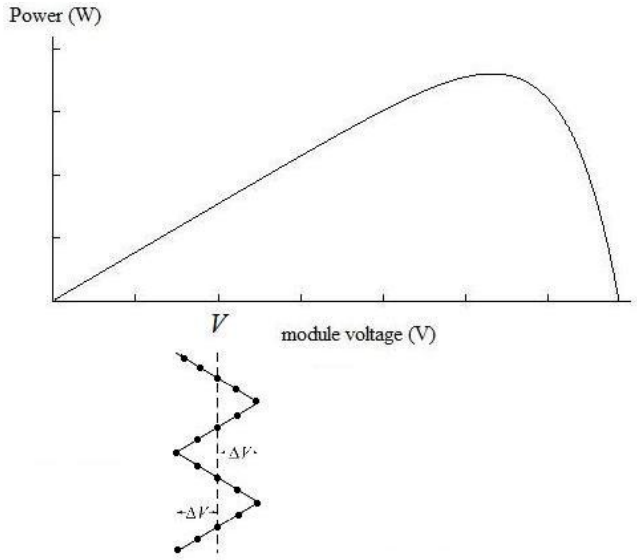

Figure 2.5: Example of dithering scheme using triangular waves

The *P&O* and *IncCond* methods are usually required to use a dithering scheme to avoid a trapped state and increase a signal-to-noise ratio (SNR). The dithering scheme is sampling a reference voltage following one or more cycles of square, sinusoidal, or triangle waves for perturbation [18, 19]. Figure 2.5 is an example of using a triangle wave for dithering. At the reference voltage *V*, the controller samples in the range from $V+\Delta V$ to $V-\Delta V$ following two cycles of the triangle wave.

Fist, this scheme increases the SNR by averaging out of noises. Under the assumption that the noises have stationary characteristics, sampling the reference *V* in the following: one cycle of the triangle wave and dividing by the number of samples is as:

$$\frac{(V+n[t_1])+\left(V+\Delta V/2+n[t_2]\right)+(V+\Delta V+n[t_3])+\left(V+\Delta V/2+n[t_4]\right)}{8}+$$
$$\frac{(V++n[t_5])+\left(V-\Delta V/2+n[t_6]\right)+(V+\Delta V-n[t_7])+\left(V-\Delta V/2+n[t_8]\right)}{8}$$
$$=V+\frac{n[t_1]+n[t_2]+n[t_3]+n[t_4]+n[t_5]+n[t_6]+n[t_7]+n[t_8]}{8} \qquad (2.6)$$

where $n[t_i], i = 1,2,\cdots,8$ is the noise at each eight different sampling time. The noises are averaged out by the dithering scheme as shown in the equation (2.6). This enables an increase the SNR by decreasing the noise signal. The dithering also reduces the risk of instant tracking failures. It consequently escapes the operating point by settling down to the opposite side of the MPP, which is called the trapped state. Figure 2.6 is the comparison of using and not using dithering in the *P&O* under a specific noisy environment. After both reach on the MPP, using dithering scheme shows better tracking performance at the steady state while the other is more unstable by noise.

However, the dithering scheme slows the tracking speed of the *P&O* system. The next perturbation command from the controller comes after finishing limited cycles of the injected dither wave. For example, if the controller samples at 100Hz without dithering, each perturbation command is derived at every 0.01s. If the controller samples at the same rates by sampling 10 points of a dither signal, the perturbation is occurred at every 0.1s ($= 0.01s \times 10$). As illustrated in Figure 2.6, the settling time when using dithering is approximately 10 times later than not using one.

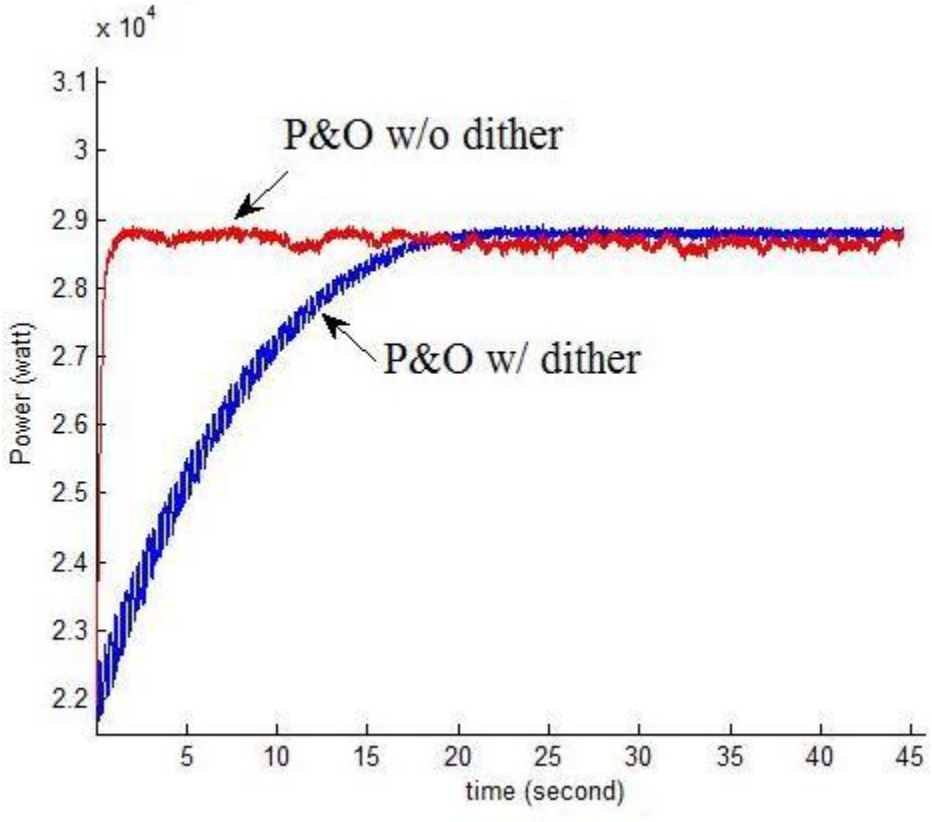

Figure 2.6: Comparison of using and not using dithering in *P&O*

Chapter 3
Proposal of New MPPT Method

3.1 General Description of Kalman Filter

Suppose that the following equations are a difference and measurement equation which the process noise $w[k]$ and the measurement noise $v[k]$ are added respectively:

$$x[k+1] = Ax[k] + Bu[k] + Gw[k] \tag{3.1}$$

$$z[k] = Cx[k] + v[k] \tag{3.2}$$

where $x[k]$ are the state and $u[k]$ are inputs. The noises are supposed to be white Gaussian and uncorrelated each other.

$$P(w) \sim N(0, Q) \tag{3.3}$$

$$P(v) \sim N(0, R) \tag{3.4}$$

where Q and R are the process noise covariance and measurement noise covariance respectively. Then two errors are defined as:

$$e[k]^{-} \equiv x[k] - \hat{x}[k]^{-} \tag{3.5}$$

$$e[k] \equiv x[k] - \hat{x}[k] \tag{3.6}$$

where $\hat{x}[k]^{-}$ is a state estimate at step k given by results from former iterations, and $\hat{x}[k]$ is a state estimation at step k given by measurement $z[k]$. The each error covariance is calculated as:

$$H[k]^{-} = E\left(e[k]^{-} e[k]^{-^{T}}\right) \tag{3.7}$$

$$H[k] = E\left(e[k]e[k]^{T}\right). \tag{3.8}$$

Measurement Update (Correct)	Time Update (Predict)
$K[k] = H[k]^{-}C^{T}\left(CH[k]^{-}C^{T} + R\right)^{-1}$ $\hat{x}[k] = \hat{x}[k]^{-} + K[k]\left(z[k] - C\hat{x}[k]^{-}\right)$ $H[k] = \left(I - K[k]C\right)H[k]^{-}$	$\hat{x}[k+1]^{-} = A\hat{x}[k] + Bu[k]$ $H[k+1]^{-} = AH[k]A^{T} + Q$

Table 3.1: Measurement and time updates in general *Kalman filter*

Table 3.1 explains processes of time and measurement updates. First, the *Kalman* gain $K[k]$ is computed from the measurement noise covariance *R* and the error covariance $H[k]^{-}$ which is estimated from one time backward in the measurement update cycle. From the computed $K[k]$, the state estimation is updated to $\hat{x}[k]$ based on the measurement $z[k]$ and the error covariance is corrected to $H[k]$. The time update predicts one time forwarding state $\hat{x}[k+1]^{-}$ and error covariance $H[k+1]^{-}$ based on the products of the measurement update: $\hat{x}[k]$ and $H[k]$. Therefore, the time update can be thought as *predictor* while the measurement update can be considered as *corrector*. As the above cycles are occurred by turns, the final estimation becomes to exclude from the noises since the error covariance $H[k]$ gets smaller and tends to approach to zero.

3.2 Noise Analysis

For realistic conditions, it is required to analysis noises in a PV system. First, there will be a mix of disturbances which are capable of interfering with the MPPT operations in the system. The disturbances are caused by thermal noise, switching noise, electromagnetic interference (EMI), and etc. The switching noise is mostly generated by switching devices such as insulated gate bipolar transistors (IGBTs), metal-oxide-semiconductor field-effect transistors (MOSFETs), or etc, and it depends on a switching

speed and size of the device. The thermal noise and EMI are also considerable disturbances in the device. Consequently, the estimation results of the controller may contain errors influenced by the disturbance. Since it is hard to determine those disturbances, it is assumed that there exist three different 1%, 0.1% and 0.01% errors which interfere with the controller's estimation in the system. From the signal viewpoint, 0.1% error means that a signal-to-noise ratio (SNR) is 1000 or 60 decibels (dB). The alternative definition of the SNR follows:

$$SNR = \frac{\mu}{\sigma} \tag{3.9}$$

where μ is mean and σ is standard deviation of the signal [20]. Accordingly, 0.01% and 1% process errors are 80dB and 40dB respectively.

Next, it is expected that errors caused by functions of both voltage and current sensors exist in the system. The voltage sensors for electronic measurements have a quantization error from resolution of an ADC. The resolution is calculated in the following:

$$\text{Re}\,solution = \frac{V_{Hi} - V_{Low}}{2^N} \tag{3.10}$$

where N is the number of bits. The common current sensors, which sometimes called to current transducers, usually have $\pm$ 1% accuracy at 25°C [21]. The $\pm$ 1% error is 100 (40dB) in SNR.

3.3 Proposed Representation

3.3.1 Adaptive MPPT Algorithm

As shown in Figure 1.2(b), the P-V characteristic of a PV array is a simple convex function with one maximum peak point. Simply, the peak point is the MPP. The

array power increases with a gradual positive slope until reaching the peak point, and decreases with a steep negative slope after passing the point.

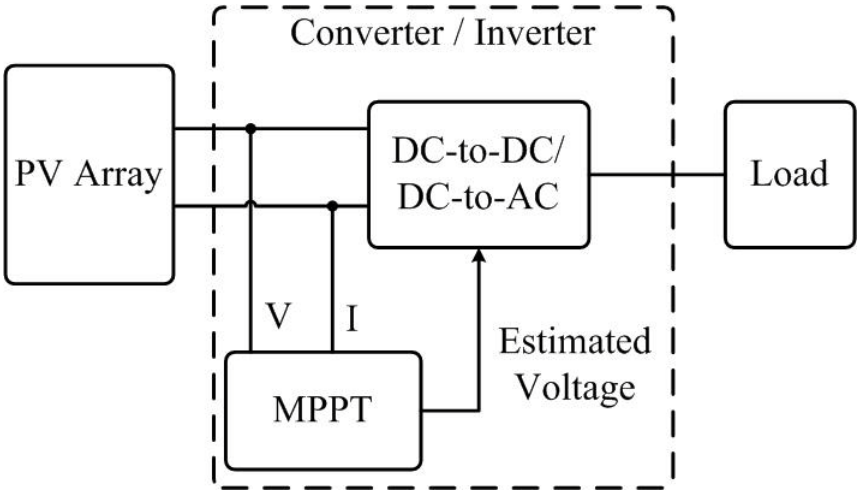

Figure 3.1: Block diagram of operation of MPPT in PV system

Based on the convex feature of the P-V characteristic, [22] proposed the tracking algorithm for a microcontroller-based design in the following:

$$V[k+1] = V[k] + M\frac{\Delta P[k]}{\Delta V[k]}, \tag{3.11}$$

where M is a step size and $\Delta P[k]/\Delta V[k]$ is an instantaneous power slope at the solar array output. A converter or inverter controller samples voltages (V) and currents (I) of the array at every sampling time, and it updates the power slope in MPPT as shown in Figure 3.1. Consequently, the estimated voltage $V[k+1]$ is derived from the updated slope at every sampling time. The instantaneous power slope can be approximately achieved by

$$\frac{\Delta P[k]}{\Delta V[k]} \approx \frac{P[k]-P[k-1]}{V[k]-V[k-1]}. \tag{3.12}$$

The MPPT algorithm using by the equations (3.11) is adapted to the microcontroller- or DSP-based designs due to its easy application to a digital design. The algorithm is also

capable of predicting the next voltage adaptively by the instantaneous power slope while the conventional methods move to the next voltage with the fixed value.

3.2.3 Proposal of New Representation

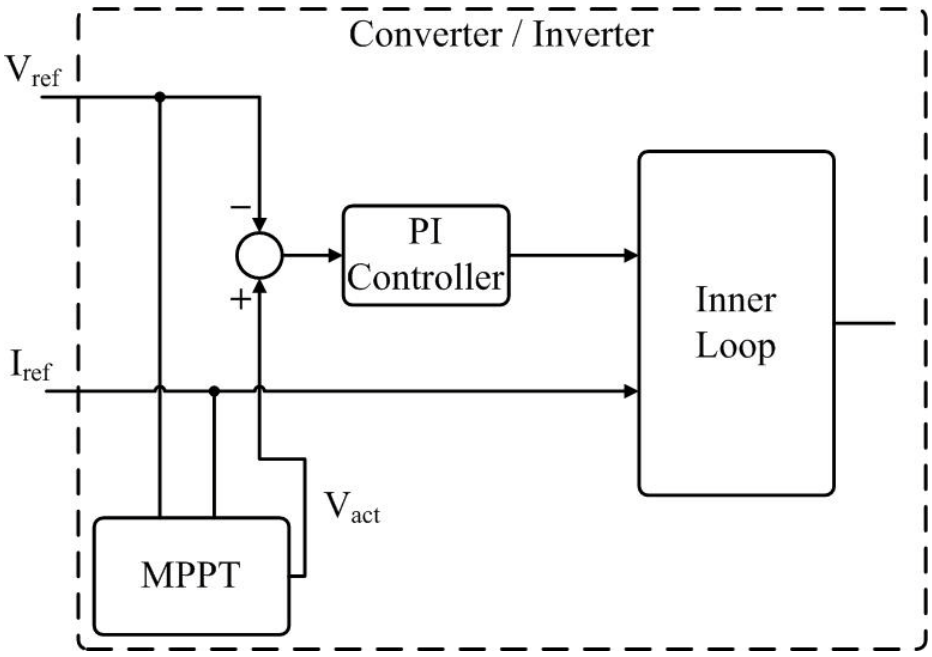

Figure 3.2: Controlling errors between actual voltage (V_{act}) and reference voltage (V_{ref})

Without errors in the system, an estimated voltage by MPPT is same with a controlled array voltage. In this case, (3.11) is written with an actual voltage V_{act} as to:

$$V_{act}[k+1] = V_{act}[k] + M \left. \frac{\Delta P[k]}{\Delta V[k]} \right|_{true}, \tag{3.13}$$

where $\left. \Delta P[k]/\Delta V[k] \right|_{true}$ is the power slope calculated by the actual voltage and current.

In the real PV system, (3.13) must consider the effects caused by the mix of the disturbances and sensor errors. When the error by the mix of the disturbances is added as $w[k]$ and the error by the sensors is considered to achieve the power slope, (3.13) can be changed to:

$$V_{act}[k+1] = V_{act}[k] + M \left. \frac{\Delta P[k]}{\Delta V[k]} \right|_{measured} + w[k], \tag{3.14}$$

where $\Delta P[k]/\Delta V[k]\big|_{measured}$ is the power slope measured by the sensors. Since the $w[k]$ is defined to 0.01%, 0.1%, or 1% errors, the computed value V_{act} [k+1] contains the corresponding percentage errors in (3.14). In addition, the power $P[k]$ is achieved by the product of sensed voltages and currents as shown in Figure 3.1, and the calculation of $\Delta P[k]/\Delta V[k]\big|_{measured}$ consequently contains the errors from both sensors' accuracies.

As illustrated in Figure 3.2, MPPT computes the input voltage of the electronic device, but there are errors by a difference between V_{act} and V_{ref}. First, (3.13) can be changed in the following:

$$V_{ref}[k+1] = V_{ref}[k] + M \left. \frac{\Delta P[k]}{\Delta V[k]} \right|_{measured}, \tag{3.15}$$

and the difference between (3.14) and (3.15) can be expressed by:

$$V_{ref}[k] - V_{act}[k] = \sum w[k], \tag{3.16}$$

where $\sum w[k]$ is the error between V_{ref} and V_{act}. The controlled value V_{ref} may not be same with the V_{act} due to various factors. One factor is assumed to disturbances in a line between the array and the power electronic device. A used proportional-integral (PI) controller also contains errors. Even without the errors from the line disturbance and PI controller in an ideal case, there is the error by the voltage sensor because MPPT recognizes the controlled voltage by sensing the voltage. Therefore, the controlled value can be represented in the following:

$$V_{ref}[k] = V_{act}[k] + v[k], \tag{3.17}$$

where $\sum w[k]$ in (3.16) is named to $v[k]$. At this point, it must be clear that MPPT does not include any process that reduces those errors directly in the system. It includes processes that reduce noise effects in only tracking computations. Therefore, the array voltage, array current, and array power oscillate in the system due to the errors.

This thesis proposes to consider the instantaneous power slope $\Delta P[k]/\Delta V[k]$ as an input signal $u[k]$ of the system. Therefore, the equation (3.14) can be assumed as one dimensional difference equation in the linear state-space representation. Both A and G in (3.1) are assumed as simply 1, and B in (3.1) is the step size M. The equation (3.17) is also assumed to the measurement equation (3.2) where $v[k]$ is the measurement noise and C is 1. Based on two known values, V_{ref} and $\Delta P[k]/\Delta V[k]\big|_{measured}$, (3.14) and (3.17) are applicable for the *Kalman filter* to estimate the state in noisy environment.

3.4 Applied Proposed Representation to Kalman Filter

From the above derived linear state-space representation (3.14) and (3.17), the *Kalman filter* can be applied to track to the MPP. The recursive computation of the filter is divided by the measurement and time update steps.

3.3.1 Measurement Update

From the error covariance $H[k]^-$ from last time update, first of all, the *Kalman* gain $K[k]$ is computed in following:

$$K[k] = H[k]^-\left(H[k]^- + R\right)^{-1} \tag{3.18}$$

where R is the measurement noise covariance. The measurement noise is assumed as disturbance which interfere an operation of both voltage and current sensors.

Next, the corrected $K[k]$ updates the estimate of $\hat{V}_{act}[k]$ given by the sensor measurement $V_{ref}[k]$ and the estimate from last time update $\hat{V}_{act}[k]^-$ like:

$$\hat{V}_{act}[k] = \hat{V}_{act}[k]^- + K[k]\left(V_{ref}[k] - \hat{V}_{act}[k]^-\right). \tag{3.19}$$

In addition, the gain $K[k]$ also updates the error covariance $H[k]$ given by the $H[k]^-$ in the following:

$$H[k] = (1 - K[k])H[k]^- . \tag{3.20}$$

3.3.2 Time Update

Based on the updated estimate $\hat{V}_{act}[k]$ and error covariance $H[k]$ of the measurement update, the succeeding estimate $\hat{V}_{act}[k+1]^-$ is projected as:

$$\hat{V}_{act}[k+1]^- = \hat{V}_{act}[k] + M \cdot \frac{P[k] - P[k-1]}{V[k] - V[k-1]} \tag{3.21}$$

with a specific step size M. $H[k+1]^-$ is also projected in the following:

$$H[k+1]^- = H[k] + Q \tag{3.22}$$

where Q is the process noise covariance of a plant.

3.3.3 Operating Summary in Proposed Method

Table 3.2 is the summary of the time and measurement updates in proposed method. From the computed *Kalman* gain, the estimated voltage and error covariance are

corrected to $\hat{V}_{act}[k]$ and $H[k]$ respectively in the measurement update. The time update estimates the forwarding voltage $\hat{V}_{act}[k+1]^-$ and error covariance $H[k+1]^-$ based on the $\hat{V}_{act}[k]$ and $H[k]$. Consequently, the estimation result $\hat{V}_{act}[k+1]^-$ is expected to be closer to a MPP than $\hat{V}_{act}[k]$ as a result of these cycles.

Measurement Update (Correct)	**Time Update (Predict)**
$K[k] = H[k]^- \left(H[k]^- + R\right)^{-1}$	$\hat{V}_{act}[k+1]^- = \hat{V}_{act}[k] + M\,\frac{P[k]-P[k-1]}{V[k]-V[k-1]}$
$\hat{V}_{act}[k] = \hat{V}_{act}[k]^- + K[k]\left(V_{ref}[k] - \hat{V}_{act}[k]^-\right)$	$H[k+1]^- = H[k] + Q$
$H[k] = \left(1 - K[k]\right)H[k]^-$	

Table 3.2: Measurement and time updates in proposed *Kalman filter*

Chapter 4
PV System Design

This thesis targets a 30kW and grid-tied PV system. Unlike a stand-alone PV system, the grid-tied PV system has an ability to feed extra generated electricity to a connected utility grid. Like most installed grid-tied systems, the targeted system is assumed to be capable of supplying all power necessary for the utility with no battery backup [2]. The size of the grid-tied system varies with many construction issues, but it mainly depends on required level of generating power. According to the U.S. solar market trend, an average non-residential size of grid-tied installations was approximately 30kW in 2004 [23].

4.1 Assumptions

Design assumptions are in following:

- Microcontrollers in both methods have identical 100Hz speed for sampling array voltages and currents.
- One recursive computation for measurement and time updates in the *Kalman filter* is executed within every 0.01 second which is the microcontroller's sampling speed.
- The estimated voltage cannot exceed $\pm$ 10V compared to the previous reference voltage in the *Kalman filter*.
- All calculation and comparisons in one *P&O* cycle are also completed within every 0.01 second.
- The *P&O* method uses a dithering scheme with a rectangular dither signal for noise reduction.

From the assumptions, the proposed controller is capable to estimate a next reference voltage in every 0.01 second. The *P&O* controller receives the voltage and power information in every 0.01 second, but it gives the estimation in every 1 second due to 100 instances of sampling per dither. In addition, the proposed controller estimates the next reference voltage adaptively while the *P&O* perturbs the voltage as a fixed value. Excessive voltage change in every 0.01 second may stress on the power electric device, and thus the voltage change is limited to $\pm$ 10V in the proposed method.

4.2 Array Design

PV panels must be linked into arrays to expect higher power than power from a single panel. A Series connection of PV panels increases array voltage up to the sum of voltages in all panels, but uniformly keeps the array current the same as the current in one panel. On the contrary, a parallel connection produces array current up to the sum of currents in all panels, but the voltage is the same as the voltage in one panel [2].

Maximum Power Voltage	55.8 V
Maximum Power Current	3.59 A
Open Circuit Voltage	68.7 V
Short Circuit Current	3.83 A
Temperature Coefficient (*V*)	-0.172 V/°C
Temperature Coefficient (*I*)	0.88 mA/°C
Maximum System Voltage	600 V

Table 4.1: Electrical specification of *Sanyo HIP-200BA19*

The PV panel selected is a *Sanyo HIP-200BA19*, which is one of common commercial panels. Table 4.1 shows key features in electrical specifications of the *Sanyo*

HIP-200BA19 under the conditions of 25°C and 1 kW/m^2 [15]. For 30kW design, 160 panels are assumed to be a combination of 8-series and 20-parallel. The 8-series connection increases the open circuit voltage (V_{OC}) of an array to 549.6V. The short circuit current (I_{SC}) is increased to 76.6A by the 20-parallel connection. From the above V_{OC} and I_{SC}, the equation (2.5) derives the P-V characteristic of the array as illustrated in Figure 4.1. The original MPP calculated from the panel combination is 32.05kW at 25°C and 1 kW/m^2, but it is decreased to 28.8kW due to the uncertain parameter *A*; this result verifies the 8 by 20 combination is acceptable to use with the 30kW design.

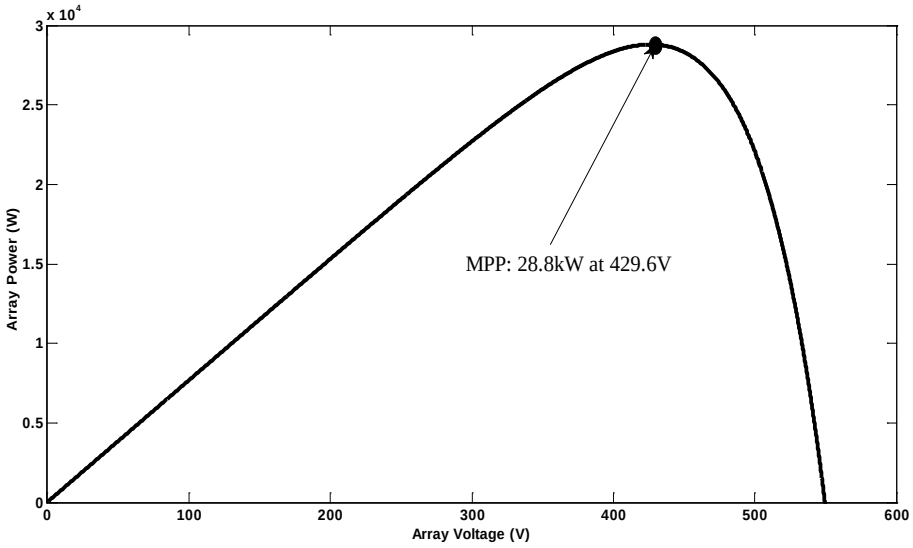

Figure 4.1: P-V characteristic of designed array at 25°C and 1 kW/m^2

4.3 Oscillation in Steady-State

It is necessary to verify the performance of the proposed method compared to other MPPT methods under specific environmental conditions. The *P&O* method is selected as a comparison target due to its popularity in industry as described in Chapter 2. The performance of the MPPT controllers may have a wide range in selected specific parameters such as an input coefficient *M* in the proposed method and a perturbation step size in the *P&O*. Those parameters have a tradeoff between a transient response and an

oscillation in the steady state. In dithering scheme, the number of samplings per one dither cycle also shows a tradeoff between a SNR and a tracking speed.

In the power viewpoint, the steady state oscillation in is expected from the standard deviation of the array power. First, the variance of the power is achieved as:

$$VAR(P) = E[P^2] - \left(E[P]\right)^2 = E[\left(VI\right)^2] - \left(E[VI]\right)^2 \tag{4.1}$$

where *P*, *I*, and *V* are the output power, the current, and the voltage from the array respectively. Since *V* contains noises as well as the output voltage, it follows:

$$V = V_O + V_P + V_M \tag{4.2}$$

where V_O is the original output voltage, V_P is the process noise, and V_M are the measurement noise. As defined in the previous chapter, the process noise is the disturbance which interferes with the estimation of the MPPT controller; the output voltage is expected to contain the process noise. Since *I* is including only the measurement noise, it can be expressed as the following:

$$I = I_O + I_M \tag{4.3}$$

where I_O is the original output current and I_M is the measurement noise. The (4.1) can be substituted to:

$$VAR(P) = E[\left(V_O + V_P + V_M\right)^2 \left(I_O + I_M\right)^2] - \left(E[\left(V_O + V_P + V_M\right)\left(I_O + I_M\right)]\right)^2. \tag{4.4}$$

Since the process noise and measurement noises are defined as following the white Gaussian distribution, V_P, V_M, and I_M are mutually independent, and their mean values are all zeros. Thereby, the (4.4) is derived as the following:

$$VAR(P) = {I_O}^2 E[{V_P}^2 + {V_M}^2] + {V_O}^2 E[{I_M}^2] + E[{V_P}^2 + {V_M}^2] E[{I_M}^2]. \tag{4.5}$$

In addition, $E[V_P{}^2]$ is equal to the process noise covariance Q as $VAR(V_P) = Q$ and $E[V_P{}^2] = VAR(V_P) + (E[V_P])^2$. $E[V_M{}^2]$ is equal to R by the same reason. $E[I_M{}^2]$ can be expressed to $VAR(I_M)$. The (4.5) is finally changed to:

$$VAR(P) = I_O{}^2(Q+R) + V_O{}^2\{VAR(I_M)\} + (Q+R)\{VAR(I_M)\}. \quad (4.6)$$

Since the measurement noise of the voltage sensor is defined to the sensor's resolution, R is expected to $(0.586)^2$ maximally. The maximal value of $VAR(I_M)$ is also expected to $(0.766)^2$ due to 1% error of the short-circuit current (I_{SC} = 76.6A). In case of 25°C and 1 kW/m^2, I_O and V_O are expected to 67.5A and 426.9V respectively. With 0.1% error (60dB SNR) of Q, the steady state oscillation will be calculated to about 1.2%.

In the *P&O*, the steady state oscillation is dependent of the dithering amount (ΔV) in Figure 2.5 as well as the perturbation step size. In general, ΔV is decided as 25% ~ 50% of the perturbation step. Therefore, all parameters in both the proposed method and *P&O* are selected to stay with the expected steady state performance, about 1.2% oscillation with 60dB process noise in the power viewpoint. Consequently, the transient response of each method becomes a significant comparison object under the same steady state performance.

4.4 Design of Proposed Method

4.4.1 Parameter Selection

In the equation (3.13), the step size M is related to a system stability [24]. The value of M has a tradeoff between a tracking speed and an oscillation range in steady state like the perturbation step size in the *P&O*. The large M improves the tracking speed because $V_{act}[k+1]$ in (3.13) is almost linearly proportional to M in a region B or C in Figure 4.2. In a region A, the difference between $V_{act}[k+1]$ and $V_{act}[k]$ would be

approaching zero as the slope $\Delta P[k]/\Delta V[k]\big|_{true}$ gradually decreases. Therefore, *M* must be selected as an appropriate value for system performance of between the steady state oscillation and the tracking speed.

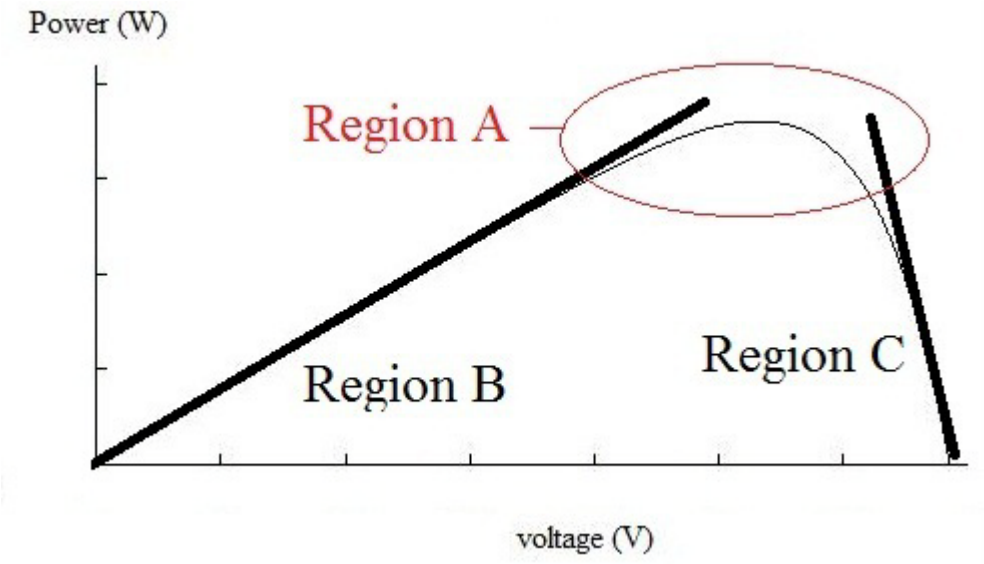

Figure 4.2: Linear and nonlinear regions of P-V characteristic

Based on the P-V characteristic in Figure 4.1, Figure 4.3 shows the change of the slope $\Delta P[k]/\Delta V[k]\big|_{true}$. The magnitude of the slope has the largest value near 0V or the open circuit voltage (V_{OC}), and it gradually approaches to zero as reaching to the MPP. The positive slope side has 67.04 by the calculation from 0V to the MPP which is 28.8kW at 429.6V. The negative slope side has -240 by the calculation from V_{OC} to the MPP. As a result of simulations, the steepest slope value is expected between -700 and -800 from an initial tracking in the negative slope side. With the design assumption that the voltage change is limited to $\pm$10V, (3.13) is changed to:

$$-10 \le V_{act}[k+1] - V_{act}[k] = M \frac{\Delta P[k]}{\Delta V[k]}\bigg|_{ture} \le 10, \qquad (4.7)$$

and *M* is limited to:

$$|M| \le \frac{10}{800} = 0.0125 \tag{4.8}$$

when the slope is the steepest. Consequently, *M* is selected to 0.125 because the lower than 0.0125 will decrease the tracking speed.

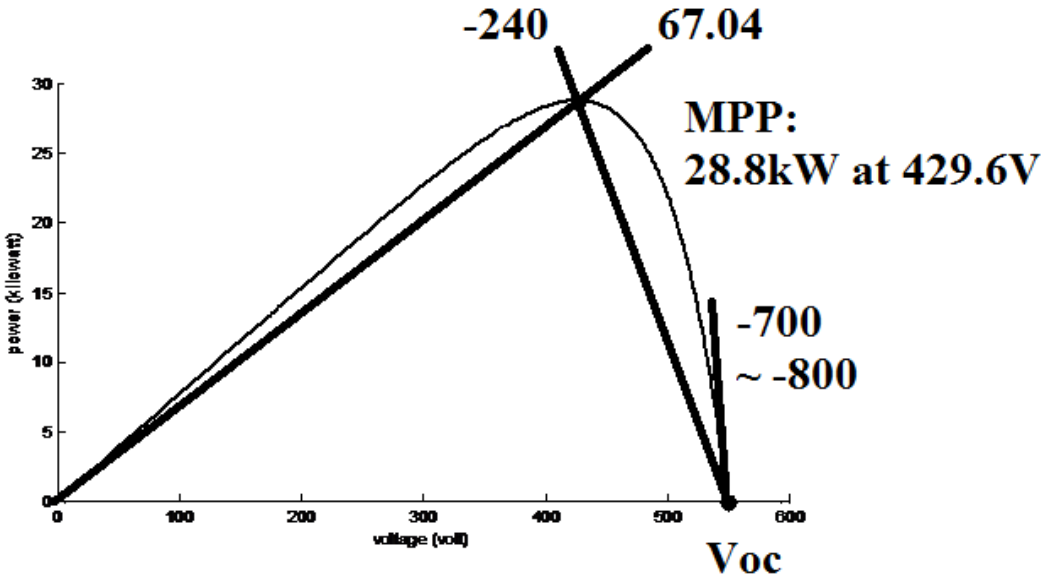

Figure 4.3: Power slope calculations based on Figure 4.1

The noise covariance *Q* and *R* are required to be decided in the *Kalman filter* design. The measurement noise covariance *R* is generally achieved from practical experiments [3]. The measurement noise is defined to the quantization error from the voltage sensor in Chapter 3. As the commercial ADC usually uses 10 bits, the voltage sensor contains about 0.098% of error which is calculated by $0.098\% \approx 100(1/2^{10})$. Therefore, *R* is 0.098% of the maximal voltage value, V_{OC}, and it is 0.29. Unlike *R*, the decision of *Q* is hard due to the difficulty of noise observation [3]. Large Q value may expect a fast filter dynamics, but has a chance to include high system noise and parameter uncertainty [25]. From the experiments, *Q* is selected to 0.3 here.

4.4.2 Performance Verification of Kalman Filter

In the real system which contains the noises, ΔP is more sensitive to noises than ΔV in the measured slope $\Delta P[k]/\Delta V[k]\big|_{measured}$ of (3.14) because ΔP includes noise from current as well as voltage. In addition, the process noise $w[k]$ in (3.14) includes 0.01%, 0.1%, or 1% calculation noises. Therefore, the estimation results are inaccurate and thus tracking failures are occurred. The noises also cause that the magnitude of the measured slope is unexpectedly changed until 10^7, which value is observed experimentally, although the largest magnitude of the true slope in (3.13) is expected between 700 and 800. The unexpected large slope is shown when ΔV becomes very small value due to the noises. On the other hand, the *Kalman filter* is assumed to have the better performance than simple adaptive equation (3.14) because of the measurement and time updates.

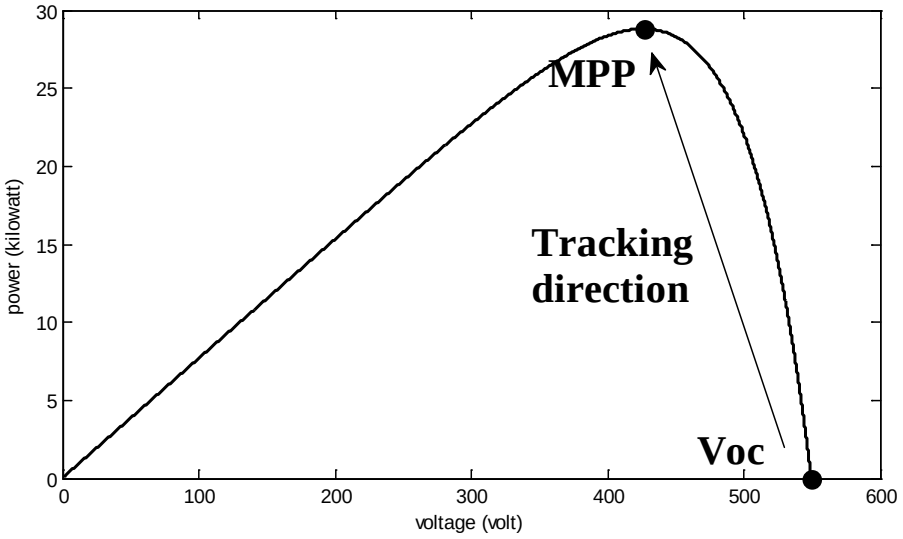

Figure 4.4: Tracking direction in P-V characteristic at 25°C and 1 kW/m^2

Figure 4.5 is a simulation result for 10 seconds between using the designed *Kalman filter* and using (3.14). The both cases start tracking from V_{OC} (549.6V) to the MPP (429.6V and 28.8kW) as shown in Figure 4.4. The simulation result plot the array power by both methods at every 0.01s. The result compares the power trajectories of the methods. The process noise is 60dB, and the environmental condition is 25°C & 1 kW/m^2.

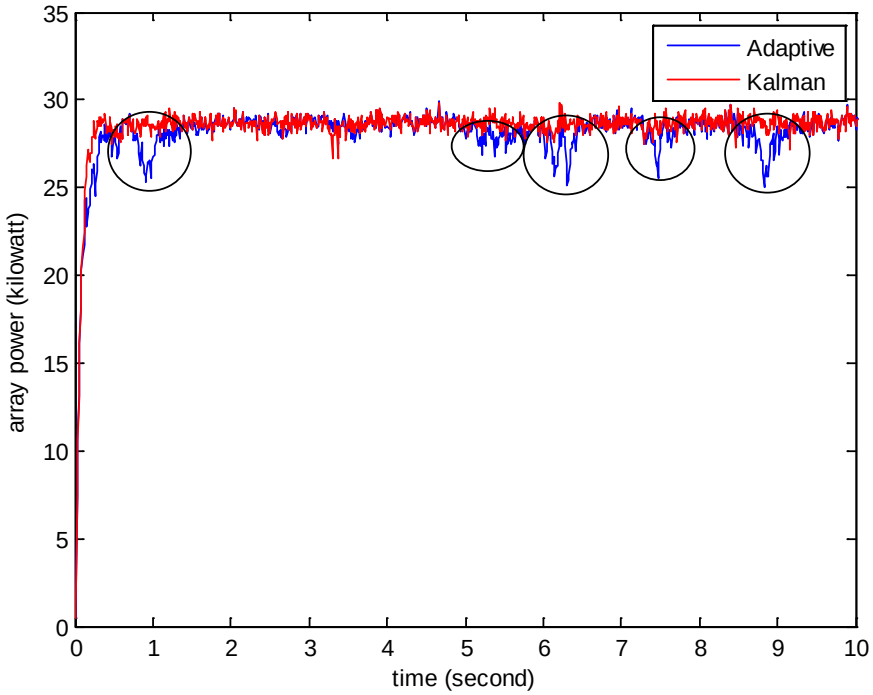

Figure 4.5: Simulation result of using designed *Kalman filter* and equation (3.14) following Figure 4.4

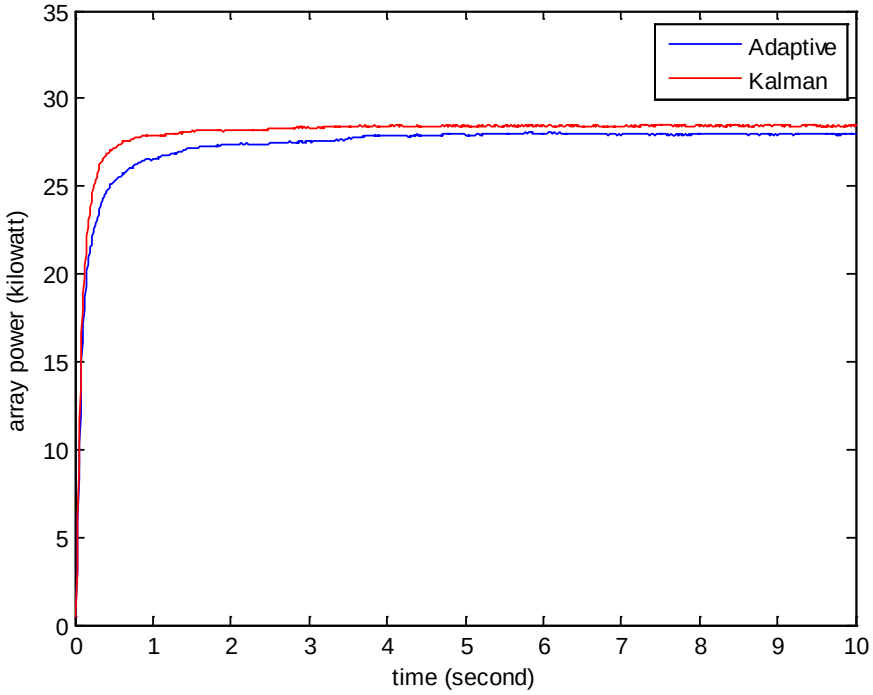

Figure 4.6: Average power values of 500 simulations following Figure 4.4

In the simulation, the voltage estimation is limited from ± 0.54V to ± 10V. The minimal limit ± 0.54V is achieved by the voltage sensor resolution, and it avoids the power slope being $\pm \infty$ which comes when ΔV is zero. The maximal limit is derived from the design assumption that the voltage change is limited to ± 10V. In Figure 4.5, using (3.14) shows momentary tracking failures as illustrated in circles, and thus it worsens the tracking behavior than using the *Kalman filter*. Since the injected noises are randomly generated following the normal distribution, only one simulation may not be difficult to compare the two methods. Therefore, Figure 4.6 is the power trajectories by averaged values from 500 simulations. Power oscillations are disappeared in the both methods due to averaging. In general, the power trajectory by using the *Kalman filter* is located highly than that by using (3.14). This result explains that the tracking failures may be occurred more in the method using (3.14), and it consequently drops the average value. The both methods show a similar performance on a transient response in Figure 4.5, but the *Kalman filter* is slightly faster in Figure 4.6 because the tracking failures are less occurred until reaching to the MPP.

4.5 Design of P&O Method

The *P&O*'s performance varies according to sampling numbers on one dithering cycle and a perturbation step size. As explained in Chapter 2, the higher the sampling numbers in the dithering the better performance against the noise effect, however it slows the tracking speed. A large perturbation step may increase tracking speed, but it causes oscillations at the steady state.

The frequency of injected dither signal may cause the distortion to the load signal. As the grid-tied load has a 60Hz frequency, the *P&O* controller is designed to sample 100 times per one dithering cycle here. Since the microcontroller samples the array voltage with 100Hz, 100 samples in the dither signal makes 1Hz frequency; 1Hz dither signal is considered to be acceptable over the 60Hz load signal. The perturbation step and the dithering amount are selected to 5V and ± 2.5V respectively. Therefore, the controller samples first 50 times at V_{ref} + 2.5V and next 50 times at V_{ref} - 2.5V with a reference voltage V_{ref} before jumping to the next reference voltage. The rectangular shape

is selected due to better performance compared to other sinusoidal and triangle shapes [19].

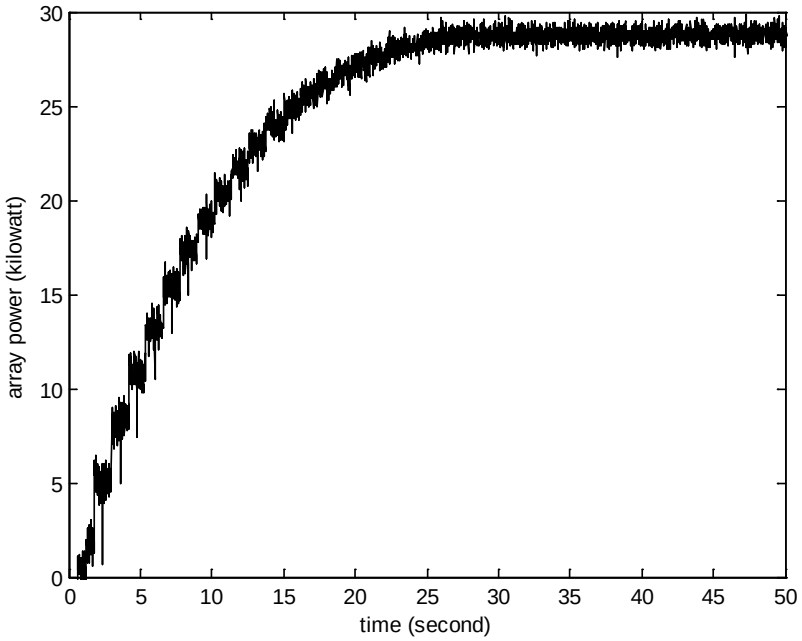

Figure 4.7: Tracking result following Figure 4.4 using designed *P&O* method

Using the suggested *P&O* design, Figure 4.7 is the tracking result during 50 seconds under the same condition with the propose method. The power from the array also stays the 1.2% oscillation range in the steady state.

Chapter 5
Simulations

All simulations have proceeded based on *MATLAB R2009b*®. For the simulation, a *PVP-30kW-LV* is selected for specifications in a PV inverter. The *PVP-30kW-LV* is designed to a single solution for a DC-to-AC power conversion in a commercial 30kW PV installation. Its maximum DC input voltage (600V) is larger than the V_{OC} of the proposed array (549.6V); the inverter is capable of connecting with the array. The inverter is able to generate power from the array in a range from 295 to 600 V. Therefore, 295V and 600V are chosen as a minimal and maximal operating points in the system respectively [26]. The inverter will be monetarily turned down during operating if the array voltage is beyond the range. In the simulations, it is assumed that the inverter is turned on without delay after the immediate turn-off.

In a real PV system, MPPT simply measures voltage and current from the PV array, and uses them to estimate a forwarding voltage in the proposed method or to decide a next perturbation direction in the *P&O*. However, the simulations need to generate the voltage and current intentionally using electrical specifications of the suggested array design. Therefore, the array's output current is decided by the equation (2.5) in the simulations based on three parameters: the load voltage, the irradiance, and the temperature. The open circuit voltage (V_{OC}) and short circuit current (I_{SC}) are 549.6V and 76.6A respectively in the equation as explained in the previous chapter.

The simulations also generate the process noise $w[k]$ and measurement noise $v[k]$ which follows a normal distribution with zero-mean. As the process noise is defined to 0.01%, 0.1%, and 1% of computing errors, a standard variation of each distribution is the corresponding percentage of V_{OC}. The measurement noise may be various as described in Chapter 3, but only the error by the voltage sensor is considered in these simulations. As the commercial ADC usually uses 10 bits, the voltage sensor contains about 0.098% of error indicated in Chapter 4. In dB scale, it is approximately 60.21dB. The resolution

becomes about 0.586V based on V_{OC}, which comes from $0.54 \approx (549.6 - 0)/2^{10}$. Therefore, a standard variation of $v[k]$ is selected to 0.54V in the simulations.

In the proposed method, the power slope (3.12) is achieved from the array voltage and current at every 0.01s. And, the next estimation is derived by the measure and time updates in one iteration cycle of the *Kalman filter*. The estimated value is limited from ± 0.54V to ± 10V compared to the previous estimation as described in the previous chapter. In the *P&O* method, following the square-waveform dithering, first the controller collects 50 voltage and current samples corresponding to 2.5V larger than the array voltage and calculates each power. Next, the controller collects 50 voltage, current, and power samples corresponding to 2.5V smaller than the array voltage. After that, the controller calculates averages of the voltages and powers of the 100 samples, and decides the perturbation direction based on comparisons of the averaged values.

The simulation results plot the array power by both MPPT methods at every 0.01s. The results compare the power trajectories of the methods from an identical start point, and the area difference of the trajectories is consequently assumed to the more generated power by the method which has the faster tracking response.

5.1 Transient Response to Sudden Changes

The object of these simulations focuses on a tracking speed until reaching on a MPP under a sudden change of environmental conditions. The first change is when the system is restarted unexpectedly, and the other is when irradiance is decreased by 50%. The faster method is considered to show the better performance because the closer the point is to the MPP the greater the ability to generate more power. Three different process noises are selected for performance comparisons. As previously mentioned, both the proposed and *P&O* methods show same steady state behavior under 60dB (0.1% error) of the process noise. Therefore, the simulations will compare the performances of the two methods via each sudden change under 10 times greater-40dB (1% error)-and 10 times less process noise-80dB (0.01% error)-as well as 60dB.

5.1.1 Sudden System Restart

A PV system is sometimes turned off suddenly and restarts the system after a momentary power failure on power devices. During the time the system is off, the array voltage usually reaches its open-circuit voltage (V_{OC}) because the PV arrays have charged gradually without power delivery to the load. Therefore, the beginning point of the tracking is usually located between an MPP and the V_{OC}; MPPT must occur in order to climb on the negative slope side of the P-V characteristic.

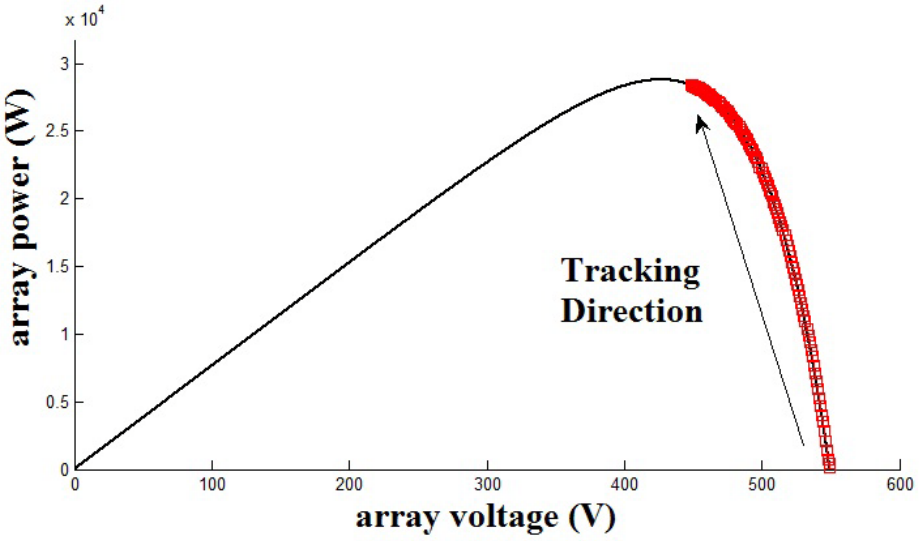

Figure 5.1: Initial 120 estimation results of proposed method in sudden system restart

The simulation supposes that the PV system is suddenly turned off and restarted at 25°C and 1 kW/m^2. The proposed and *P&O* controllers begin tracking from the open-circuit voltage (549.6V) at the same time. Figure 5.1 shows the initial 120 tracking results of the proposed method under 60dB process noise. Each square box in Figure 5.1 indicates an estimation result derived from an iteration of the *Kalman filter*.

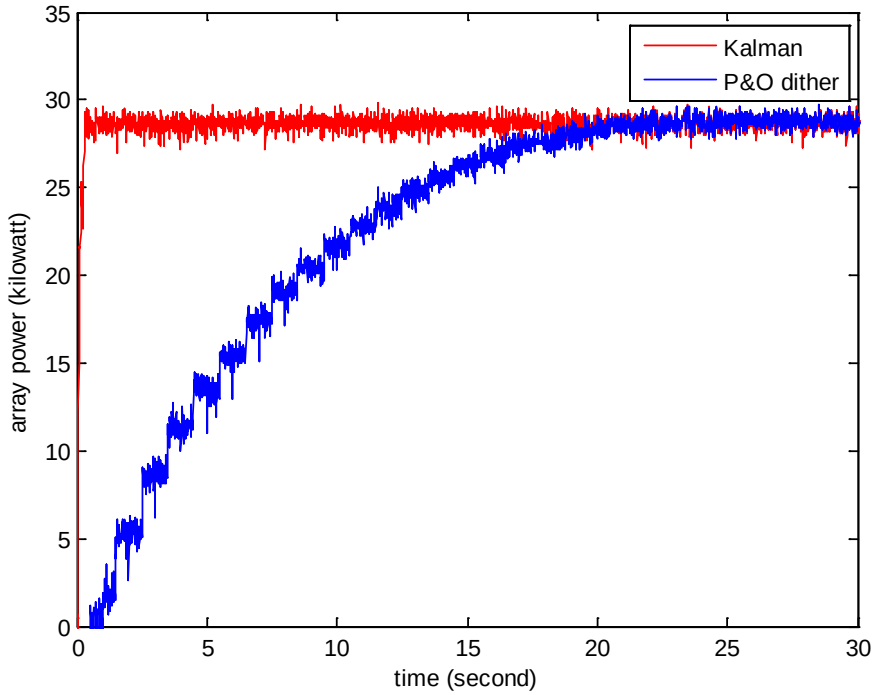

Figure 5.2: Simulation result of sudden system restart under 60dB process noise

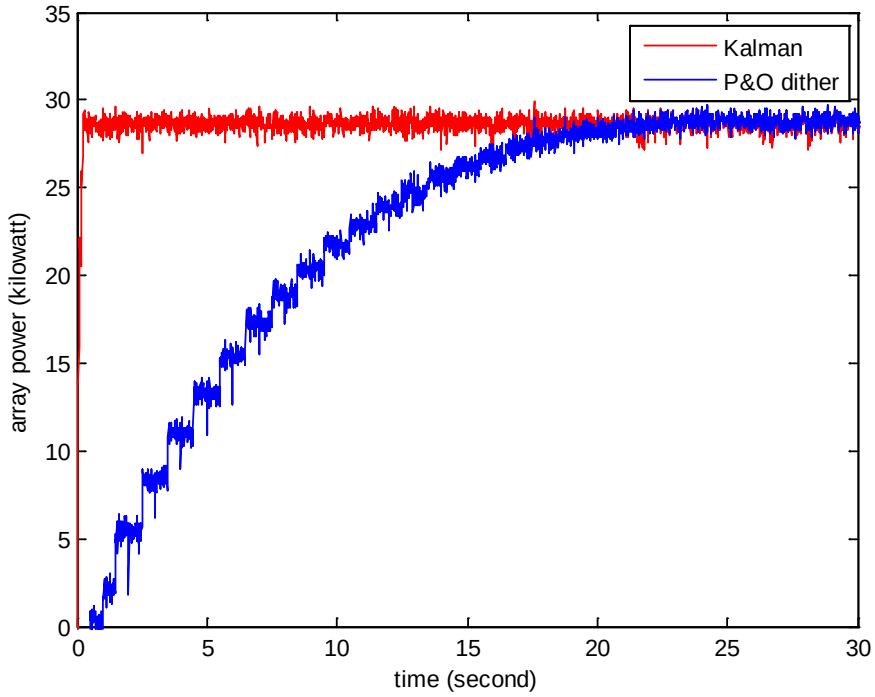

Figure 5.3: Simulation result of sudden system restart under 80dB process noise

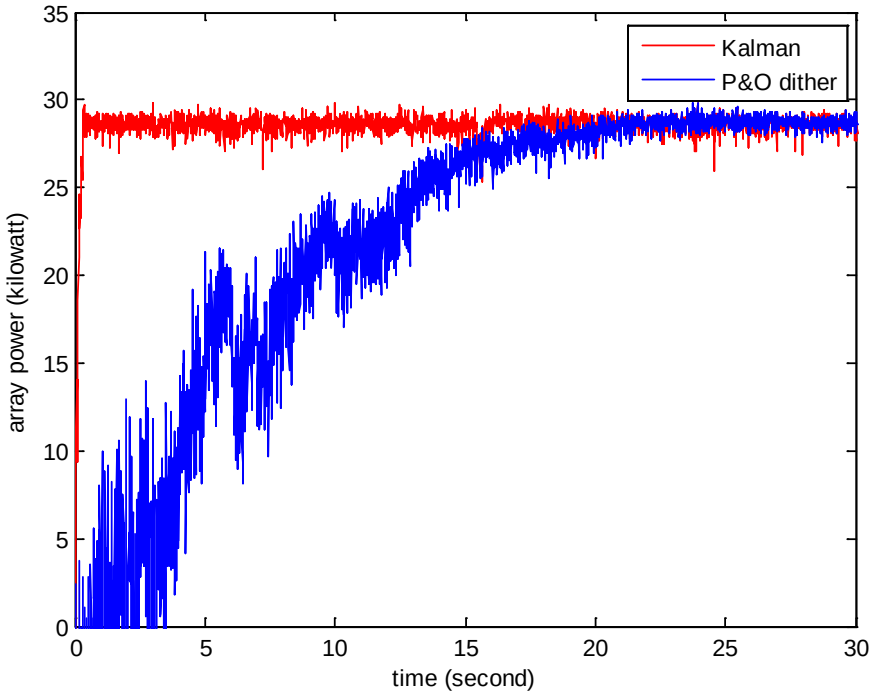

Figure 5.4: Simulation result of sudden system restart under 40dB process noise

Figure 5.2 and 5.3 are simulation comparisons of the proposed method and the *P&O* method for 30 seconds under 60dB SNR and 80dB SNR of the process noise respectively. In both cases, the proposed method reaches the MPP-28.8kW-less than a second while the *P&O* takes between 20 and 25 seconds. Figure 5.4 is the simulation result under 40dB SNR. The proposed method also shows much faster tracking speed like the two other cases.

5.1.2 Sudden Irradiance Changes

PV arrays are very sensitive to rapid environmental changes. The array's irradiance dependence is especially notable as described in chapter 2. When the irradiance is suddenly changed, the P-V characteristic of the array and its MPP are simultaneously reformed. Therefore, the MPPT controller is required to track the changed MPP as soon as possible.

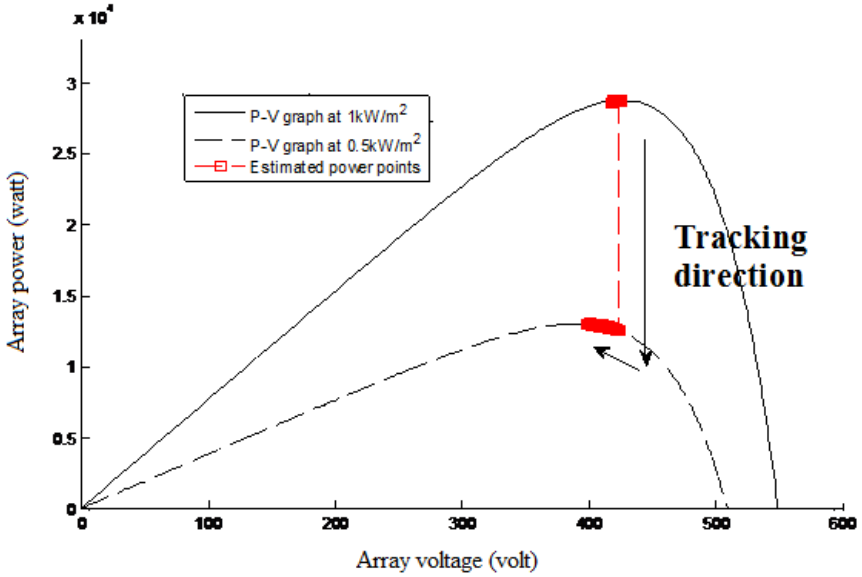

Figure 5.5: Middle 200 estimation results of proposed method before and after irradiance change

In [27], 50% shadow effect is used as a simulation method to verify tracking performances of MPPT algorithms. Therefore, it is assumed that the irradiance is suddenly reduced from 1 kW/m^2 to 0.5kW/m^2 at a specific time (30 seconds) with no temperature change. In Figure 5.5, a solid line and dotted line are the P-V characteristics at 1 kW/m^2 to 0.5kW/m^2 respectively. The square boxes are 200 estimation results by the proposed method before and after the shadow effect. The MPP is moved from 28.8kW at 429.6V to 13.1kW at 391.2V by the shadowing.

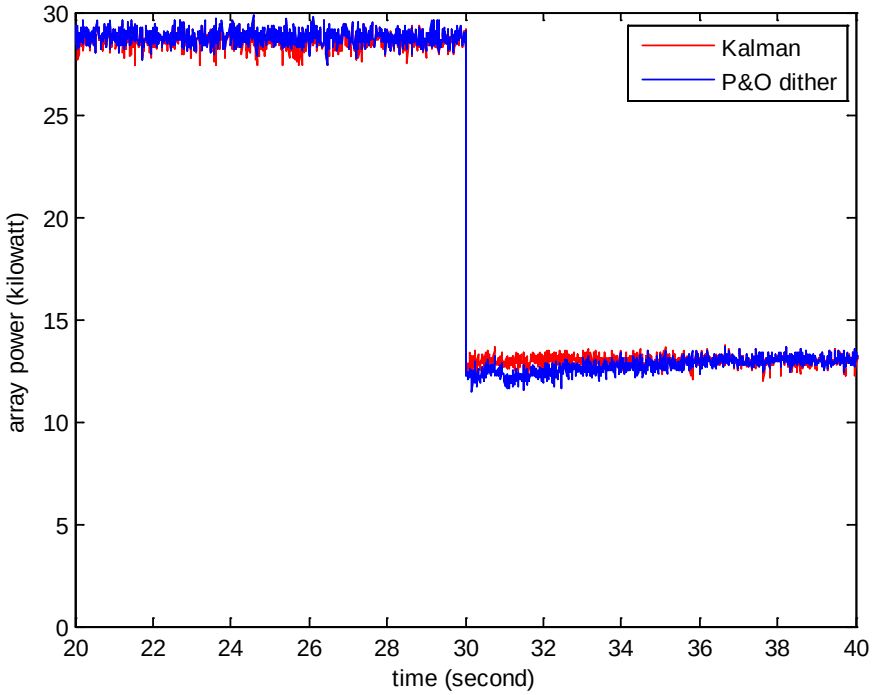

Figure 5.6: Simulation result of 50% decrease of irradiance under 60dB process noise

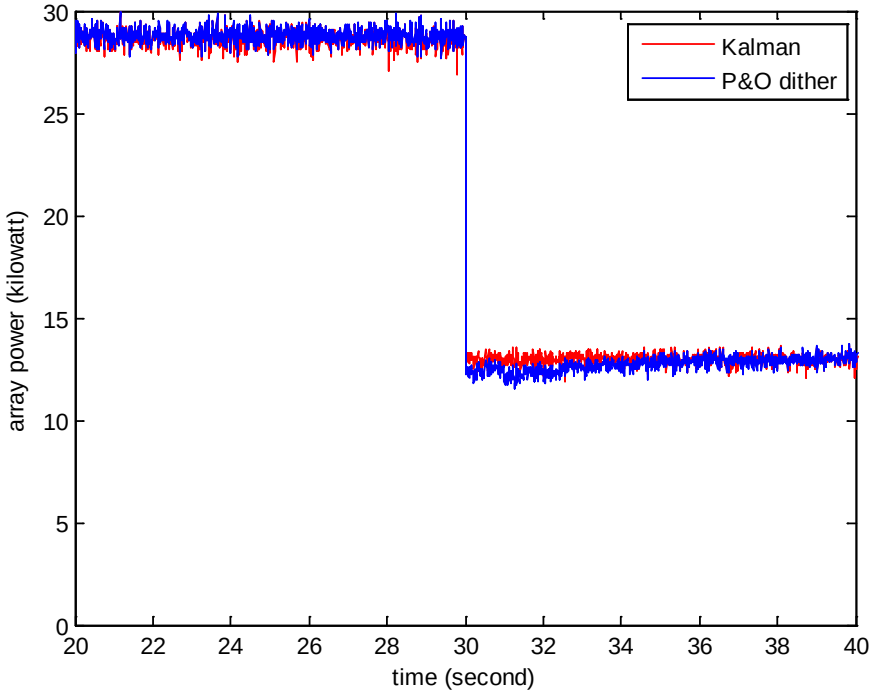

Figure 5.7: Simulation result of 50% decrease of irradiance under 80dB process noise

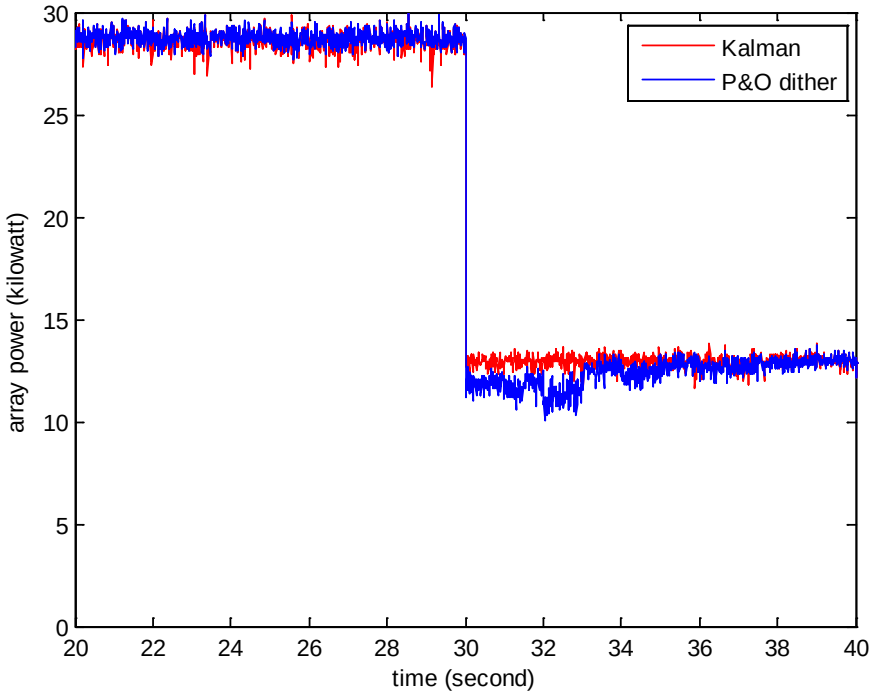

Figure 5.8: Simulation result of 50% decrease of irradiance under 40dB process noise

Figure 5.6, 5.7, and 5.8 illustrate the tracking performances of the proposed and *P&O* method between 20 and 34 seconds when 50% decrease of irradiance occurs at 30 seconds under 60dB, 80dB, and 40dB SNR process noises respectively. The proposed method tracks on the MPP less than 1 second while the *P&O* takes about 4 seconds for the three cases.

5.1.3 Summary of Sudden Changes

The results of the simulations vary due to the noises which are randomly generated in each simulation. Therefore, all achieved numbers are the average values from 500 simulations.

Table 5.1 is the transient response of the proposed and the *P&O* on the two different scenarios and three noise levels. The transient response denotes the overall tracking time in seconds from the starting point to the MPP. In each scenario and at each noise level, the proposed method shows the faster transient response than the *P&O*.

Transient Response (second)						
SNR / Scenario	80dB		60dB		40dB	
	Kalman	P&O	Kalman	P&O	Kalman	P&O
System Restart	0.83	25.10	0.98	26.30	1.02	27.60
50% Irradiance Decrease (Shadowing)	0.62	9.60	0.69	11.10	0.77	13.40

Table 5.1: Transient response comparison of two methods in each scenario and noise level

In the same scenario, the proposed method shows a similar performance over the different noises. The process noise covariance Q is related to the filter dynamics [25]. Since Q is fixed, the filter has same performance over the noises. The *P&O* also shows a similar performance over the different noises, but it slightly slower in the higher noise. This is expected due to the fact that the transient response of the *P&O* much depends on the number of sampling in dithering than the noise. In the both methods, the slower response in the higher noise is assumed to be caused by the high occurrence rate of tracking failures.

Array Output Power over 1 minute Under 60dB SNR (percentage)		
Scenario / Ratio	System Restart	50% Irradiance Decrease (Shadowing)
$\frac{Kalman - P\&O}{P\&O}(\%)$	+ 12.20%	+ 0.054%

Table 5.2: Generated power comparison of two methods over 1-min in each scenario

Table 5.2 shows the comparison of the accumulated output powers over a specific time. The environmental condition is limited only to 60dB process noise, 25°C, and 1 kW/m^2. For one minute, the proposed method is expected to generate 12.20% and 0.054% more when the scenario of 'System restart' and '50% Irradiance decrease' respectively over the *P&O* method. It is simply explained by the faster tracking response of the proposed method as shown in Table 5.1.

From the above simulations, the proposed method is expected to have a transient response advantage under any sudden environmental or system change compared to the *P&O*. It means the proposed method may deliver more power than the *P&O* from the array to power electronic devices under the changes.

5.2 Daily Generation

The other simulation target is observing amounts of generated power from the array during one day. As shown in Chapter 2, PV arrays show a much higher dependence on irradiance than on temperature. Therefore, only a daily irradiance change is postulated in the simulations. The process noise is selected to 60dB only for both the proposed and *P&O* method. As shown in Figure 1.7 and 1.8, irradiance data is utilized from the SRRL BMS [11]. The irradiance used is the Direct-normal irradiance (DNI) with 1-minute time interval.

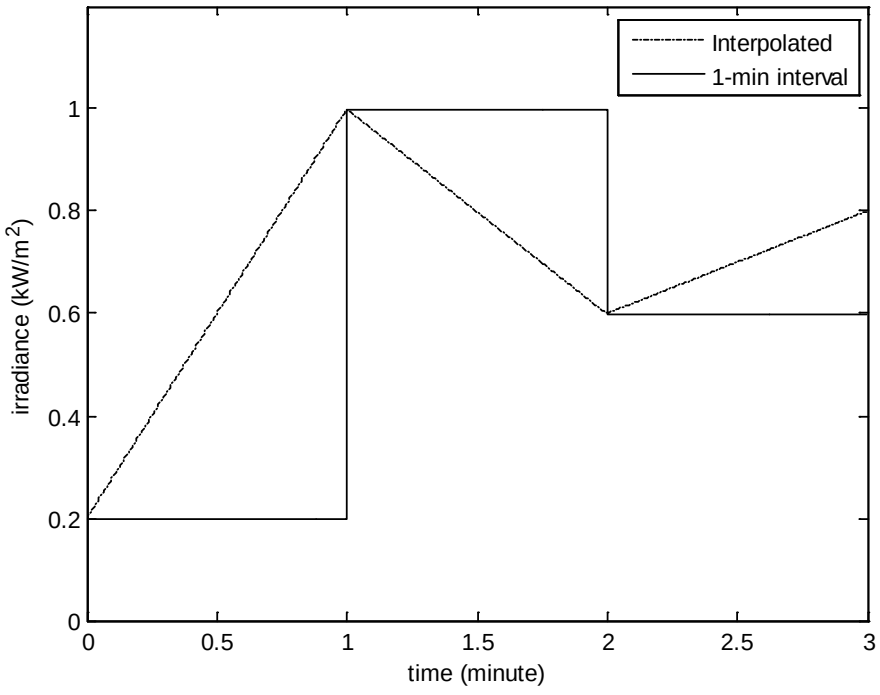

Figure 5.9: Example of difference between 1-min interval and interpolated irradiance data

Even though the 1-minute data is the shortest time interval from the SRRL BMS, it may be considered to be unrealistic for the daily simulation because 1 minute is longer than the sampling speed of the MPPT controller: 0.01 second. For alternative numerical analysis of the data, linear interpolation is used to cut the irradiance data from the 1-minute to 0.010-second interval. Figure 5.9 illustrates a difference between original 1-minute interval data and interpolated result. When the 1-minute irradiance data is supposed to change as 0.2 kW/m^2 → 1 kW/m^2 → 0.6 kW/m^2 → 0.8 kW/m^2 for 3 minutes, the interpolated result shows the gradual changes linearly. However, the interpolated result is still containing unrealistic factors because it does include dynamic irradiance changes. In real system, the irradiance may be fluctuated several times for 1 minute, but the interpolated result is always changed gradually. This thesis used both the original 1-minute interval data and the interpolated result for the daily simulation.

5.2.1 Smooth Irradiance Changes

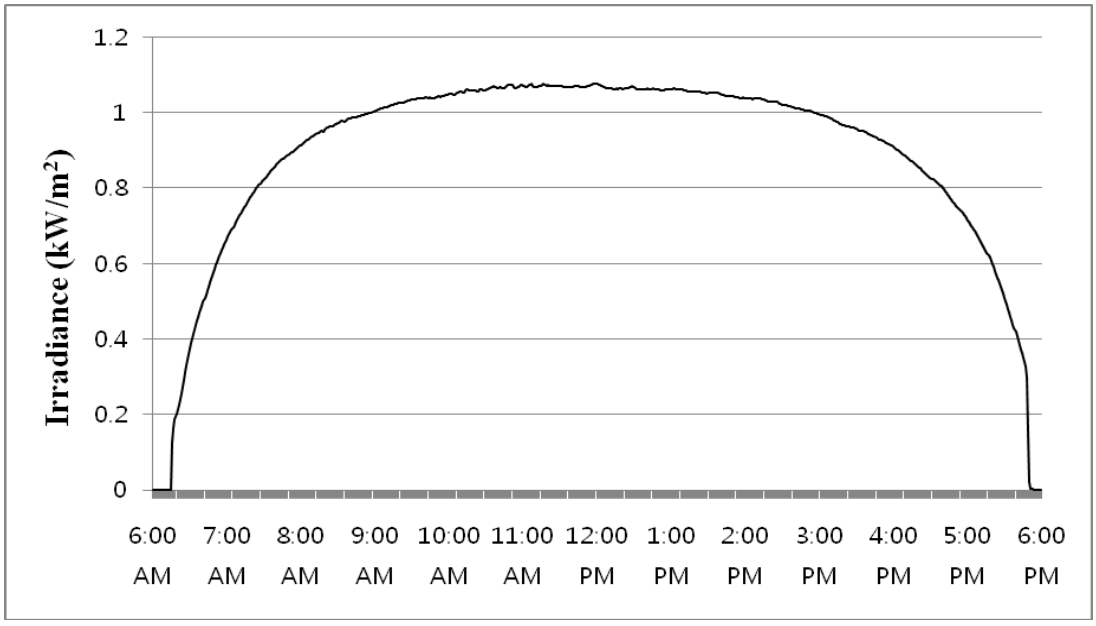

Figure 5.10: Irradiance data on March 14, 2009

To select specific days and their DNI data, daily irradiance changes are observed for the entire month of March, 2009. Figure 5.10 is plotted by the 1-minute interval irradiance data on March 14, and it is same to Figure 1.7(n). The sun rose at 6:16 AM

and set at 5:55 PM in that day. There is no severe irradiance change during that period; the irradiance is gradually increased and decreased from sunrise to sunset. Thus, March 14 may be considered as one of the best cases for the PV generation.

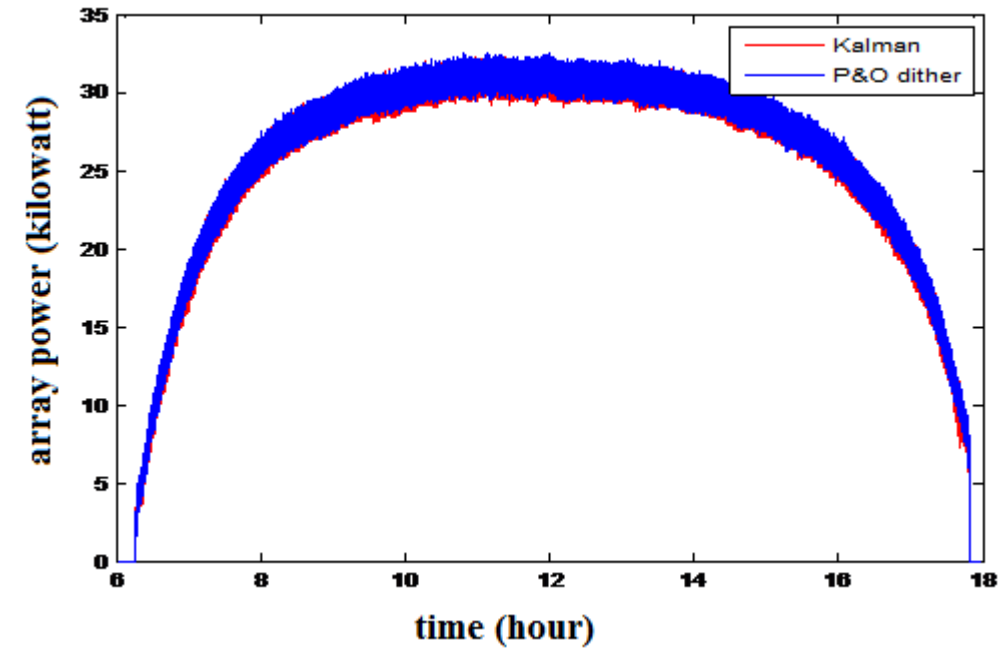

(a) 1-min interval irradiance data

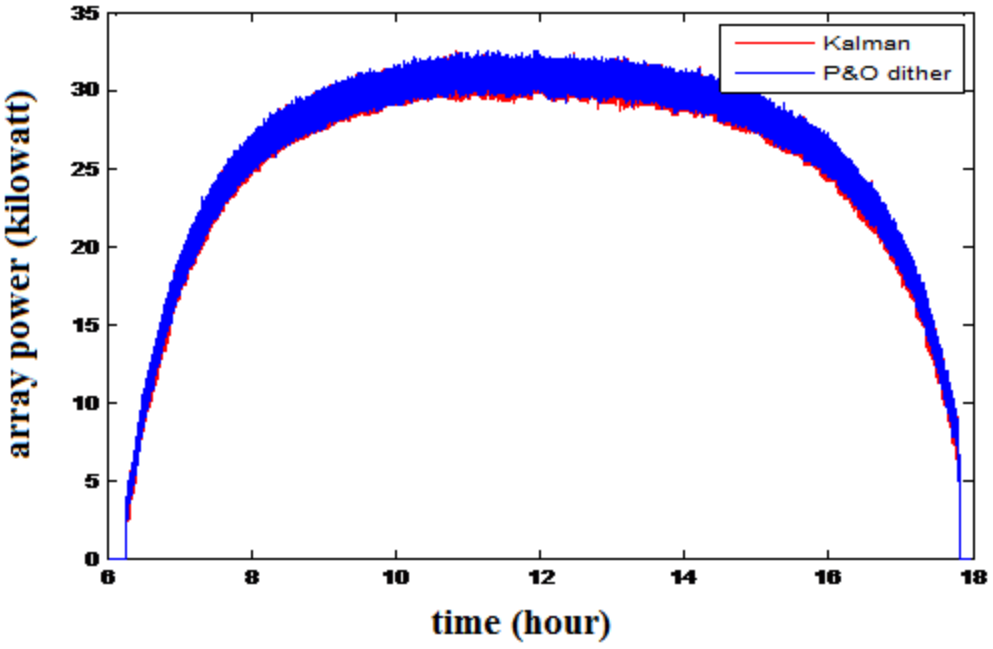

(b) Linearly interpolated irradiance data

Figure 5.11: Simulation results of daily generation on March 14, 2009

Figure 5.11(a) and (b) are the simulation results of daily generation on March 14 based on the original 1-minute interval irradiance and linearly interpolated irradiance respectively. From both figures, two methods show similar performances over one day.

In this case, the proposed method is anticipated to have advantages when the system initiates. The PV inverter is assumed to operate in the range between 295V and 600V. After the sun rises, the inverter does not start operation until the array voltage reaches on the above range. Except the sunrise, the tracking speed is not primarily considered on that case because there are not seen sudden irradiance changes during that day.

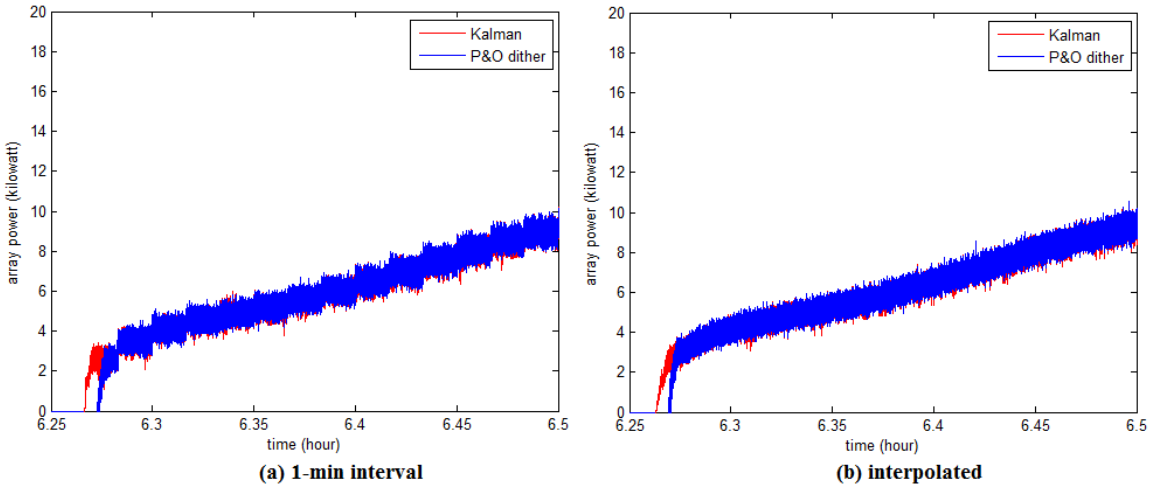

Figure 5.12: Simulation results limited to between 6:15 AM and 6:30 AM on March 14, 2009

Figure 5.12(a) and (b) are focused on the limited time between 6:15 AM and 6:30 AM in Figure 5.11(a) and (b) respectively. The both methods initiate tracking several minutes later after sunrise when the array voltage is over the threshold voltage of the inverter. From both figures, the proposed method shows the faster tracking performance than the *P&O*.

5.2.2 Severe Irradiance Changes

Figure 5.13 is the irradiance change of March 25 as same with Figure 1.8(j). There are more than 40 examples of the irradiance changes larger than 200W/m^2 and

some as great as 500W/m^2 occurred 6 times. It is assumed that there would be dynamic environment changes during that day. The transient response of the MPPT method is mostly dominant in the system performance in this case. Therefore, the proposed method is expected to have advantages in every irradiance change as well as the sunrise compared to the *P&O*.

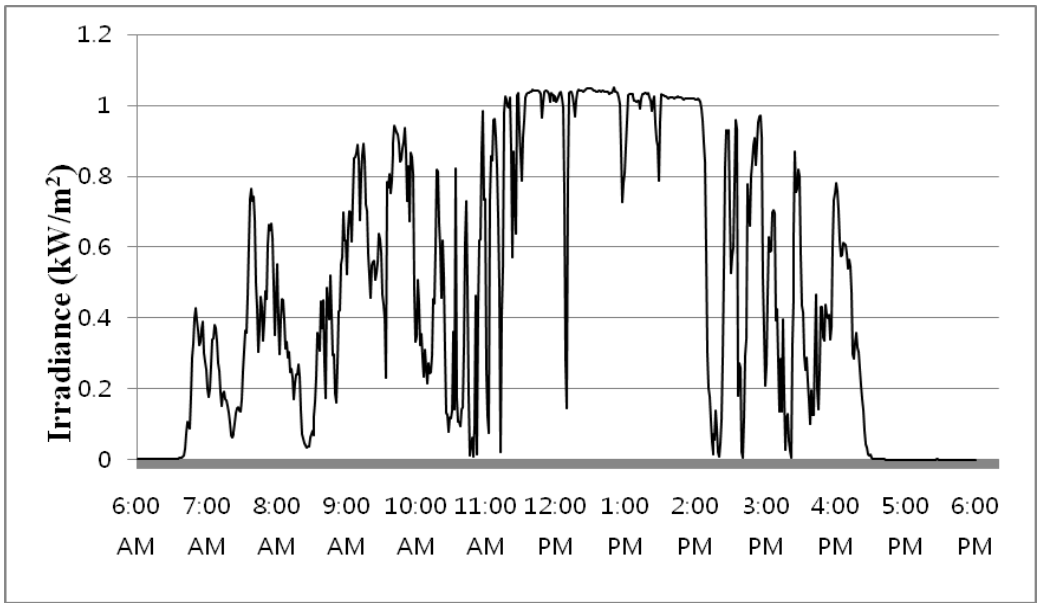

Figure 5.13: Irradiance data on March 25, 2009

Figure 5.14(a) and (b) illustrate the simulation results of daily generation on March 25 based on the original 1-minute interval irradiance and linearly interpolated irradiance respectively. For specific observation of the simulation results, the results are limited to the time period between 10:45 AM and 11:15 AM. Figure 5.15(a) and (b) are focused on the limited time in Figure 5.14(a) and (b) respectively. For 30 minutes, the irradiance is fluctuating with a large variance, and consequently the PV system is turned off and restarted 4 times repeatedly due to the fluctuation. Whenever the system restarts, the proposed method shows the faster transient response than the *P&O* in the both simulations. In the comparison of 1-minute interval and linearly interpolated irradiance data, the proposed method shows the better performance on using the 1-miunte interval. It is expected due to the fact that the 1-miunte interval irradiance data contains more

dynamics. The irradiance is changed momentarily per minute in the 1-minute interval, and the proposed method has an advantage on the irradiance dynamics.

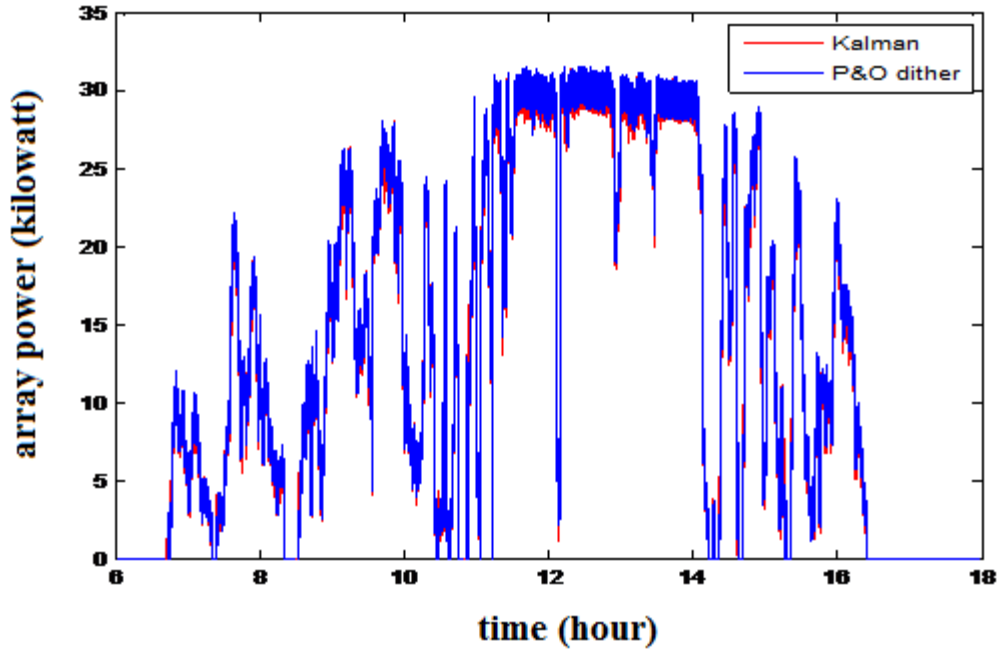

(a) 1-min interval irradiance data

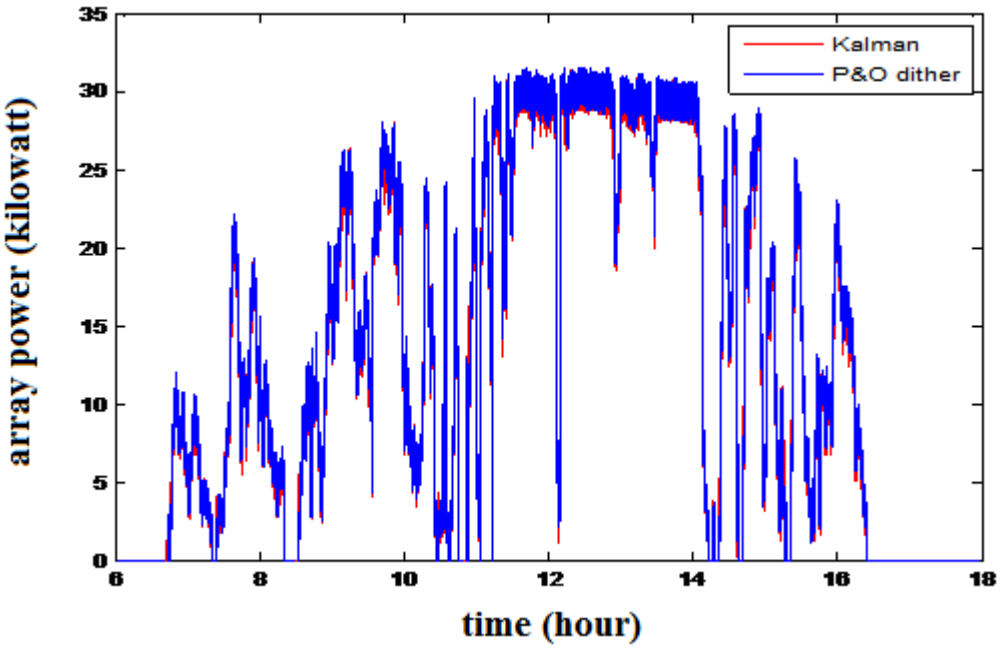

(b) Linearly interpolated irradiance data

Figure 5.14: Simulation results of daily generation on March 25, 2009

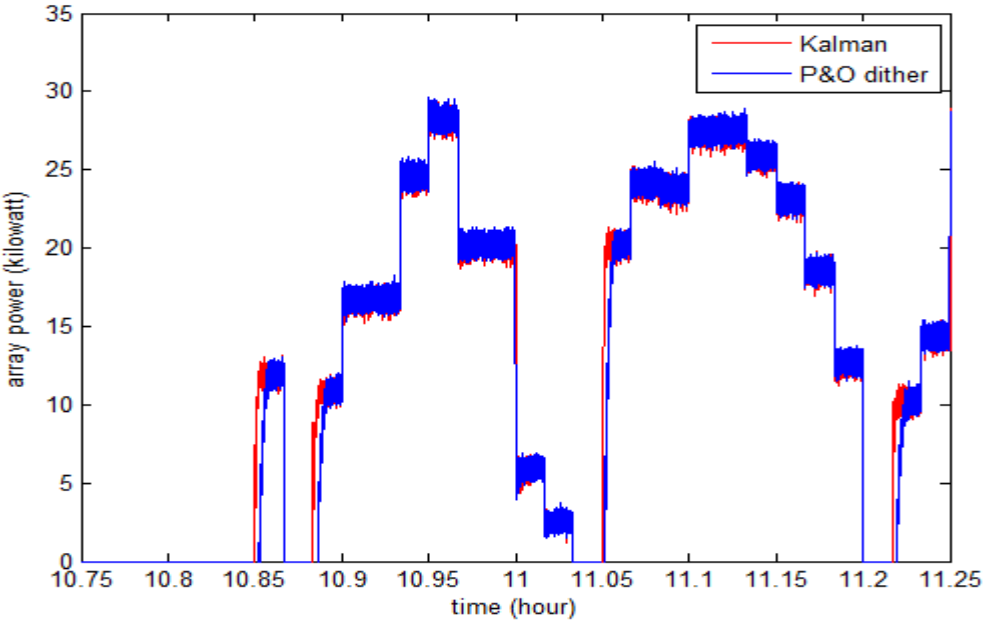

(a) 1-min interval

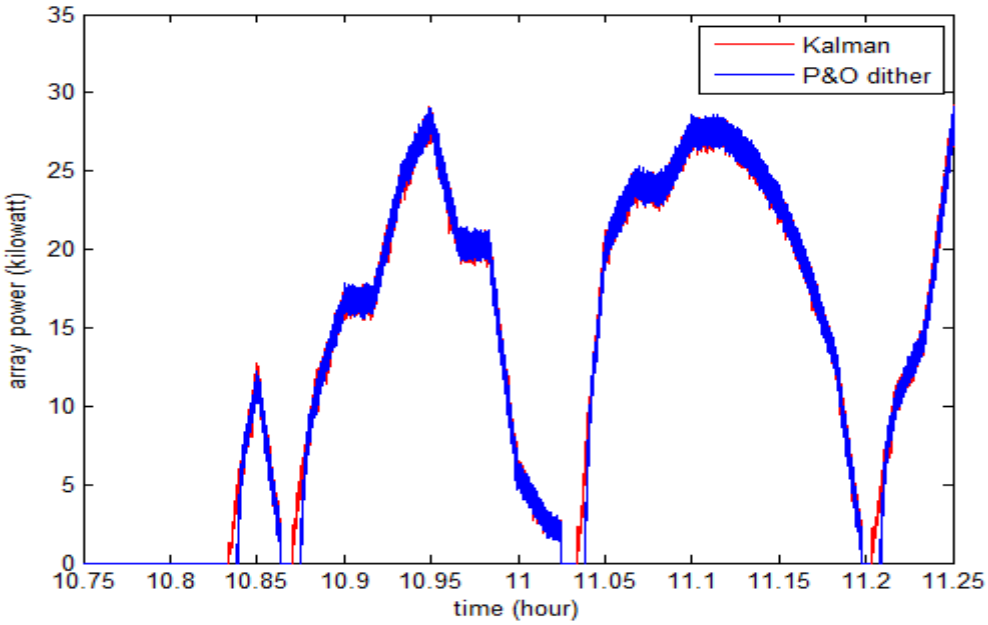

(b) Interpolated

Figure 5.15: Simulation results limited to between 10:45 AM and 11:15 AM on March 25, 2009

5.2.3 Summary of Daily Generation

All achieved numbers are the average values from 10 simulation iterations. Table 5.3 and 5.4 show the comparison of the accumulated output powers over one day based on the 1-miute interval and linearly interpolated irradiance data respectively.

Array output power over one day with 1-min interval irradiance		
Date / **Ratio**	**March 14, 2009 (Smooth changes)**	**March 25, 2009 (Severe changes)**
Kalman – P&O (kWh)	+ 0.08 kWh	+ 1.31 kWh
$\frac{Kalman - P\&O}{P\&O}(\%)$	0.00%	+ 0.83%

Table 5.3: Generated power comparison of two methods in each day based on 1-min interval data

Array output power over one day with interpolated irradiance		
Date / **Ratio**	**March 14, 2009 (Smooth changes)**	**March 25, 2009 (Severe changes)**
Kalman – P&O (kWh)	+ 0.07 kWh	+ 1.01 kWh
$\frac{Kalman - P\&O}{P\&O}(\%)$	0.00%	+ 0.64%

Table 5.4: Generated power comparison of two methods in each day based on interpolated data

In case of smooth irradiance changes, March 14, the two methods show the similar performance in both Table 5.3 and 5.4. The approximately 0% difference in both results are assumed that the more power of the proposed method, 0.08kWh and 0.07kWh, is too small compared to overall daily accumulated power. However, the proposed method generates 1.31kWh (0.83%) more in Table 5.3 and 1.01kWh (0.64%) more in Table 5.4 under severe irradiance changes, March 25. The proposed method has an advantage of the fast transient response, and it consequently generates more power than the *P&O* under the dynamic irradiance changes. As expected in Figure 5.15, the

proposed method shows the better performance in the simulation using the 1-minute interval data than the interpolated data due to more dynamics in the 1-minute interval data.

Expected cost advantage of the proposed method (U.S. dollar)				
Date / **Used data**	**March 14, 2009 (Smooth changes)**		**March 25, 2009 (Severe changes)**	
1-min interval	Denmark	U.S.	Denmark	U.S.
	\$0.03	\$0.01	\$0.52	\$0.14
Linearly interpolated	Denmark	U.S.	Denmark	U.S.
	\$0.03	\$0.01	\$0.40	\$0.11
2009 U.S. Average Price Per Kilowatt-hour is \$0.11				
2009 Denmark Average Price Per Kilowatt-hour is \$0.40				

Table 5.5: Expected cost advantage of proposed method per day (Denmark & U.S.)

Table 5.5 compares the cost advantage of the proposed method base on Table 5.3 and Table 5.4. The U.S. and Denmark are selected as reference countries. According to the U.S. Energy Information Administration, the average residential price per kilowatt-hour in 2009 is \$0.11 and \$0.40 in the U.S. and Denmark respectively [28]. Based on the prices, the proposed method is expected to earn \$0.40 ~ \$0.52 more in Denmark and \$0.11 ~ \$0.14 more in the U.S. when the condition of severe environmental changes. Even though those monetary values may be not significant in the 30kW PV system, the higher profit is expected in several hundred kilowatts size of large commercial PV systems or several megawatts size of solar farms.

Chapter 6
Conclusion and Future Works

6.1 Conclusion

This thesis proposes a MPPT algorithm using the *Kalman filter* for a PV system. P-V characteristic of a PV array is a simple convex shape with one maximum peak point. Based on the characteristic feature, it has introduced a MPPT algorithm that forwarding voltage estimation is performed by an addition between present voltage data and an instantaneous power slope. MPPT using this algorithm is able to estimate the voltage adaptively. However, the slope calculation contains noise effect in a real system, and the slope is getting sensitive as approaching to a MPP. A process noise also disturbs the estimation of the introduced adaptive algorithm. Thus, using the *Kalman filter* based on the adaptive algorithm is able to reduce tracking failures by the noises. This thesis assumes the power slope as an input signal in the system, and the adaptive MPPT equation consequently becomes one dimensional difference equation with adding process noise. A measurement equation is derived by adding measurement noise to the state. The *Kalman filter* is applied to the proposed linear state-space representation, the difference and measurement equations.

The P-V characteristic of the array is dependent of environmental conditions, especially temperatures and irradiances. When the sudden environmental condition changes are occurred frequently, transient response of the MPPT algorithm is a key factor to improve the performance. Besides, some conventional MPPT algorithms use a dithering scheme in order to reduce noise effects, however it slows the transient response of the algorithms. The *Kalman filter* keeps dynamic performance of the adaptive equation in the noisy environment. Therefore, the proposed MPPT method is expected to have an acceptable performance on the sudden environmental condition changes with noises.

A 30kW grid-tied PV system is designed in this thesis with both the proposed and *P&O* MPPT controllers. An array design is introduced by using a specific PV panel, *Sanyo HIP-200BA19*. The process and measurement noises are analyzed by possible disturbances, sensor accuracy, ADC resolution, and etc. In the proposed MPPT controller, the parameter *M*, *Q*, and *R* are selected by practical experiments or theoretical approaches for performance. The performance of the *P&O* method depends on a perturbation step size and dithering amount. In this thesis, the two controllers are designed to have a similar performance in the steady state; the transient response becomes a dominant factor on system performance as the result.

Simulations are performed by comparisons of the proposed and *P&O* methods divided into sudden changes in three different noise levels. The proposed method has showed the advantage on the transient response compared to the *P&O* in the simulations. The simulations are also performed by comparisons of the two methods using real irradiance data for two entire days, one day is smooth irradiance changes and the other day is severe irradiance changes. The proposed method has showed the better performance when the irradiance is severely fluctuating than the *P&O* while the two methods have showed the similar performances on the smooth irradiance changes.

6.2 Future Works

- Implementing the proposed algorithm in a real microcontroller-based PV system,
- Comparing performances of the two methods under a condition that irradiance and temperature are changed continuously not minutely,
- Trial to use an *Extended Kalman filter* (EKF) considering nonlinearity of array characteristics caused by uncertainties,
- Applied to mobile-based PV systems which need fast MPPT relatively due to movements,
- And advanced analysis of process and measurement noises in a PV power electronic device.

Chapter 7

References

[1] P. Lynn, *Electricity from Sunlight: An Introduction to Photovoltaics*: Wiley, 2010.

[2] R. Messenger and J. Ventre, *Photovoltaic systems engineering*: CRC, 2004.

[3] G. Welch and G. Bishop, "An introduction to the Kalman filter," *University of North Carolina at Chapel Hill, Chapel Hill, NC,* 1995.

[4] S. Julier and J. Uhlmann, "A new extension of the Kalman filter to nonlinear systems," 1997, p. 26.

[5] MathWorks. R2010 Documentation - kalman [Online]. Available: http://www.mathworks.com/help/toolbox/control/ref/kalman.html

[6] R. Kalman, "A new approach to linear filtering and prediction problems," *Journal of basic Engineering,* vol. 82, pp. 35-45, 1960.

[7] L. Levy, "The Kalman filter: Navigation's integration workhorse," *GPS World,* vol. 8, pp. 65-71, 1997.

[8] R. Engle and M. Watson, "The Kalman filter: Applications to forecasting and rational expectations models," 1987, p. 281.

[9] R. Gencay, *et al.*, *An introduction to wavelets and other filtering methods in finance and economics*: Academic Pr, 2002.

[10] C. Chui and G. Chen, *Kalman filtering: with real-time applications*: Springer Verlag, 2009.

[11] N. S. R. R. Laboratory. [Online]. Available: http://www.nrel.gov/midc/srrl_bms/

[12] N. Mutoh, *et al.*, "A method for MPPT control while searching for parameters corresponding to weather conditions for PV generation systems," *IEEE Transactions on Industrial Electronics,* vol. 53, pp. 1055-1065, 2006.

[13] Y. Jung, *et al.*, "Improved perturbation and observation method (IP&O) of MPPT control for photovoltaic power systems," 2005, pp. 1788-1791.

[14] T. Markvart, *Solar electricity*: John Wiley & Sons Inc, 2000.

[15] SANYO, "HIT Photovoltaic Module," H. P. datasheet, Ed., ed, 2008.

[16] T. Esram and P. Chapman, "Comparison of photovoltaic array maximum power point tracking techniques," *IEEE Transaction on Energy Conversion,* vol. 22, pp. 439-449, 2007.

[17] F. Liu, *et al.*, "Comparison of P&O and hill climbing MPPT methods for grid-connected PV converter."

[18] N. Pongratananukul, "Analysis and simulation tools for solar array power systems," University of Central Florida Orlando, Florida, 2005.

[19] A. Sinha and P. Chadha, "Investigation on the effect of various dithers in a noisy communication channel," 2002, pp. 924-927.

[20] J. Bushberg, *et al.*, "The essential physics of medical imaging," *Medical Physics,* vol. 30, p. 1936, 2003.

[21] LEM, "Current Transducer HTA 100 .. 1000-S," H.-S. datasheet, Ed., 6 ed, 2009.

[22] P. Huynh and B. Cho, "Design and analysis of a microprocessor-controlledpeak-power-tracking system [for solar cell arrays]," *IEEE Transactions on Aerospace and Electronic Systems,* vol. 32, pp. 182-190, 1996.
[23] L. Sherwood and I. Council, "US Solar Market Trends," 2007, p. 909.
[24] E. Koutroulis, *et al.*, "Development of a microcontroller-based, photovoltaic maximum powerpoint tracking control system," *IEEE Transactions on Power Electronics,* vol. 16, pp. 46-54, 2001.
[25] S. Bolognani, *et al.*, "Extended Kalman filter tuning in sensorless PMSM drives," 2002, pp. 276-281.
[26] PVPowered^{TM}, "PVP-30kW-LV," P.-k.-L. datasheet, Ed., ed, 2008.
[27] J. Choi, *et al.*, "Tracking system and MPPT control for efficiency improvement of photovoltaic," 2008, pp. 1341-1344.
[28] U. S. E. I. Administration. Electricity Prices for Households [Online]. Available: http://www.eia.doe.gov